Int J Earth Sci (Geol Rundsch) (2016) 105:439–462
DOI 10.1007/s00531-015-1173-3

ORIGINAL PAPER

# Sedimentary development and correlation of Late Quaternary terraces in the Kyrenia Range, northern Cyprus, using a combination of sedimentology and optical luminescence data

**Romesh N. Palamakumbura[1] · Alastair H. F. Robertson[1] · Tim C. Kinnaird[2] · David C. W. Sanderson[2]**

Received: 7 October 2014 / Accepted: 16 March 2015 / Published online: 2 April 2015


**Abstract** This study focuses on the younger of a series of Quaternary terraces along the flanks of the Kyrenia Range in northern Cyprus, specifically the Kyrenia (Girne) and the Koupia terraces. The Kyrenia (Girne) terrace is tentatively correlated with oxygen isotope stage 5 (125 Ka), and the Koupia terrace with oxygen isotope stage 3 (<50 Ka). Along the northern flank of the range, the Kyrenia (Girne) terrace deposits (5–20 m above modern sea level) typically begin with a basal lag conglomerate and then pass upwards into shallow-marine calcarenites and then into variable aeolianites, paleosols and fluvial deposits (up to 20 m thick). In contrast, the Koupia terrace (<2 m above modern sea level) consists of aeolianites and shallow-marine calcarenites (up to 8 m thick). The equivalent deposits along the southern flank of the range are entirely non-marine fluvial mud, sands and conglomerates. The marine to continental terrace systems can be tentatively correlated based on mapping, height above modern sea level and sedimentary facies. However, variable preservation and patchy exposure require such correlations to be independently tested. To achieve this, a portable optically stimulated luminescence (OSL) reader was used to determine the luminescence characteristics of the two terrace systems. Luminescence profiles show major differences in luminescence characteristics between the two terrace depositional systems, which can be related to sedimentary processes, provenance and age. These features allow sections in different areas to be effectively correlated. Individual sections show luminescence properties that are generally consistent with an expected up-sequence decrease in age. However, the younger Koupia terrace deposits show higher luminescence intensities compared with the older Kyrenia (Girne) terrace deposits. This can be explained by multiple phases of reworking of the Kyrenia (Girne) terrace deposits, which changed the luminescence characteristics of the sediment. The use of the portable OSL reader is therefore an effective means of correlating Late Quaternary terrace deposits in northern Cyprus and probably also elsewhere.

**Keywords** Field sedimentology · Portable OSL reader · Northern Cyprus · Late Quaternary terraces · Luminescence data · Tectonic uplift

## Introduction

Recent years have seen an increasing amount of research focussed on the processes and timing of surface uplift, ranging from the scale of coastal uplift to mountain uplift. The Eastern Mediterranean is a favoured region for such studies, for example the extension-related coastal uplift of the Gulf of Corinth in Greece (e.g. Leeder et al. 2003). Within Anatolia and the easternmost Mediterranean region, there is considerable interest in the uplift of southern Turkey and the Anatolia plateau, in specific areas (e.g. Ecemiş Fault Zone; Jaffey and Robertson 2004) and also regionally (Göğüş and Pysklywec 2008; Dilek and Sandvol 2009; Cosentino et al. 2011; Schildgen et al. 2012). Syn-collisional break-off of the northward subducting African plate has been proposed as the key driving factor of the vertical uplift of the Taurides (Schildgen et al. 2012). However, it is also suggested that the collision of the Eratosthenes Seamount with the Cyprus trench to the south of Cyprus was a key driving mechanism in the uplift of the Troodos Massif, Cyprus, and this could be an additional factor in regional-scale uplift (Robertson

✉ Romesh N. Palamakumbura
rpalamakumbura@gmail.com

[1] Grant Institute, The King's Buildings, James Hutton Road, Edinburgh EH9 3FE, UK

[2] SUERC, Rankine Avenue, East Kilbride G75 0QF, UK

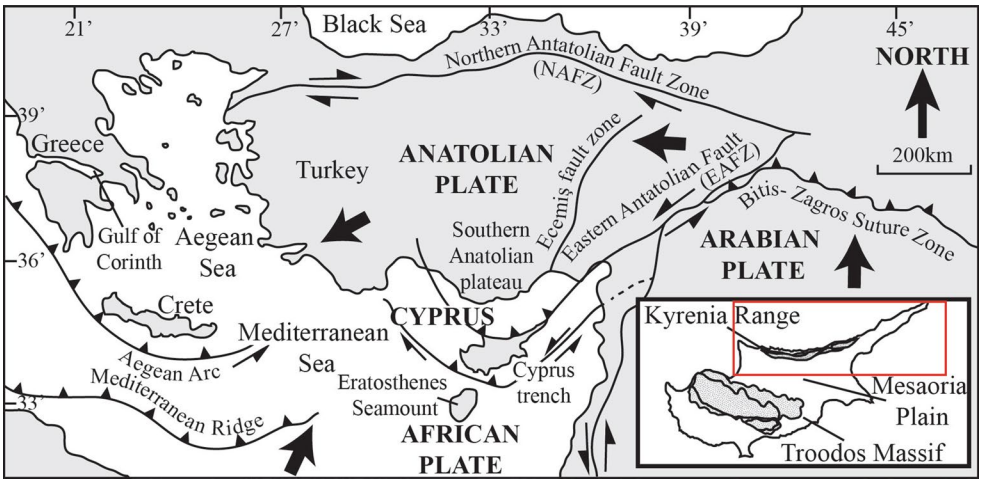


**Fig. 1** Tectonic setting of the eastern Mediterranean during the Plio-Quaternary, modified from Robertson and Xenophontos (1993). Study area shown by *rectangle*

2000; Schildgen et al. 2012; Fig. 1). The domal uplift was potentially aided by the effects of serpentinisation of the mantle wedge beneath the Troodos Massif (Robertson 1990, 1998; Poole and Robertson 1991).

The uplift of the Troodos Massif is known from research on the Plio-Quaternary deposits exposed in the south of Cyprus. This effectively began with mapping of the deposits by the Cyprus Geological Survey Department (e.g. Bagnall 1960) and early stratigraphical studies (Ducloz 1964). This was supplemented by sedimentological and dating studies (Poole et al. 1990; Poole and Robertson 1991, 1998, 2000), allowing a tectonic-sedimentary model for the uplift to be proposed. Recently, the deposits have been dated using a combination of magnetostratigraphy (Kinnaird et al. 2011), optically stimulated luminescence (OSL) and isotopic studies (Harrison and Newell 2004, 2013; Kinnaird and Robertson 2013). Different areas, for example south-eastern Cyprus (Harrison et al. 2012), central southern Cyprus (Kinnaird and Robertson 2013) and western Cyprus (Kinnaird and Robertson 2013; Zomeni, unpublished PhD thesis, 2012; Weber et al. 2011), have distinctive tectonic and sedimentary features related to the Quaternary uplift such that individual areas need to be carefully studied before the overall regional uplift can be understood.

An important question is how the uplift of the Troodos Massif compares in timing and process with the uplift of southern Anatolia. The two regions are separated by the approximately E–W trending Kyrenia Range in northern Cyprus, which is the main focus of this paper. The Kyrenia Range is known to have undergone strong uplift during the Plio-Quaternary (Ducloz 1972; Baroz 1979; Robertson and Woodcock 1986). Quaternary deposits have been mapped on both sides of the Kyrenia Range and a series of geomorphological terraces, and related deposits have been recognised (Ducloz 1963; Knupp 1964).

Detailed understanding of the uplift of the Kyrenia Range requires modern sedimentological studies and dating of the Quaternary deposits exposed on both flanks of the Kyrenia Range. Also, the existing mapping and correlation of the terraces around both flanks of the range (Ducloz 1963; Knupp 1964; Baroz 1979) need to be tested. Our main aims here are first to provide an outline description and interpretation of the sedimentology of the two topographically lowest, and by inference youngest, terrace deposits that are exposed along both the northern and the southern flanks of the range. The main aim of the sedimentological study is to describe the sedimentary sequences, internal sediment facies, sediment composition, provenance and diagenesis. Secondly, we aim to correlate the two lower terrace systems along both flanks of the range using the luminescence properties within and between the two terrace systems utilising a portable OSL reader. Such correlations, once established, can be combined with absolute age dating (work in progress), to provide a basis for testing alternative models of the uplift of the Kyrenia Range in its regional tectonic setting.

## Regional setting

The Kyrenia Range has undergone overall tectonically driven uplift during the Plio-Quaternary from below sea level in the Pliocene to c. 1000 m above modern sea level (AMSL) today (Dreghorn 1978; Baroz 1979; Robertson and Woodcock 1986; Kempler and Ben-Avraham 1987; Palamakumbura 2015). The series of geomorphological terraces along the northern and southern flanks of the range are believed to have developed during the Quaternary time interval (Ducloz 1963, 1972; Knupp 1964; Moshkovitz 1966; Dreghorn 1978; Baroz 1979; Robertson and Woodcock 1986; see Fig. 2).

Our field investigations show that the deposits associated with the Kyrenia (Girne) and the Koupia terrace systems have a patchy distribution along the northern coast, occasionally extending up to c. 1 km inland. Previously, the terraces were correlated and assigned to temporal subdivisions mainly based

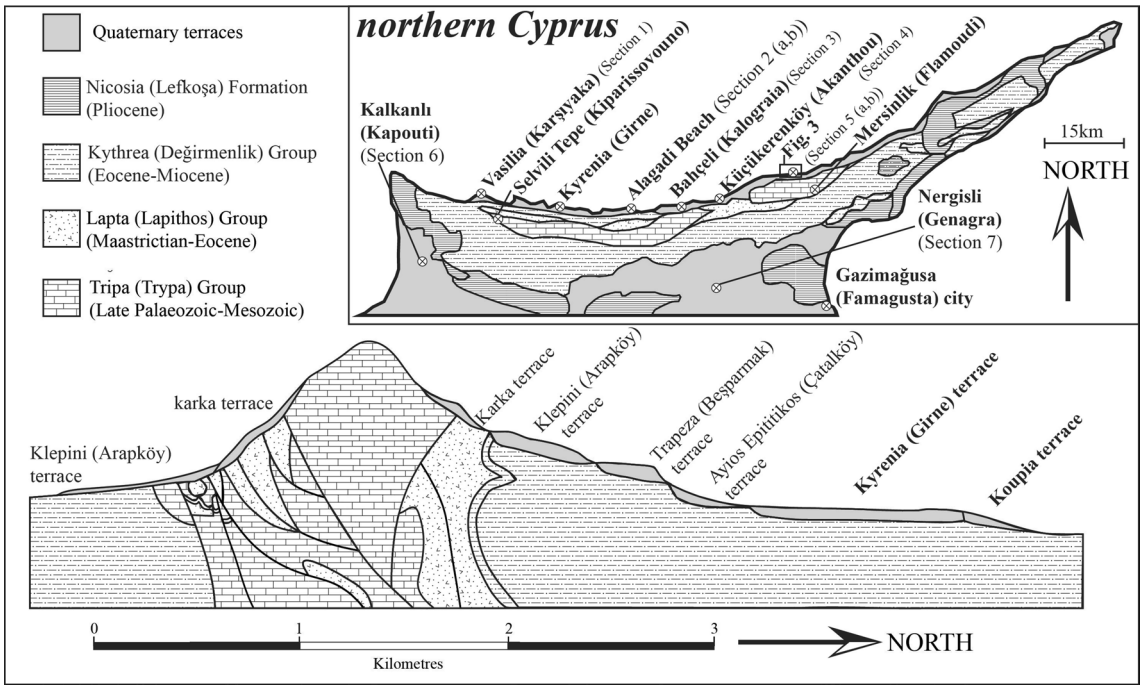


**Fig. 2** Simplified geological cross section through the central part of the Kyrenia Range (based on Baroz (1979), Robertson and Woodcock (1986) and McCay and Robertson (2012)) showing the relative positions of the Quaternary terraces. The *inset* sketch shows a summary geological map of northern Cyprus with the main localities and towns marked

on their height above modern sea level (Ducloz 1963; Baroz 1979). However, this does not take account of sedimentological evidence that the terraces may dip seawards from proximal to distal settings. In principle, terraces of the same relative age can occur at different topographical heights above sea level in different outcrops. It is also possible that faulting could have offset terraces of different ages. For example, the Koupia terrace deposits are discontinuously exposed along the coast, which in principle could be caused by patchy deposition, variable preservation or the effects of faulting. Prior to any quantitative work on the timing of uplift of the terraces, it is, therefore, essential to establish the basic sedimentary characteristics and the lateral correlations of the two terrace systems.

Non-marine terraces are present in places along the southern flank of the range. These terraces were partially mapped and correlated with the marine terraces along the southern flanks of the range by Ducloz (1963), again based mainly on relative topographical height. However, these terraces are patchily exposed and spatially isolated from the terraces along the northern flank of the range.

## Underlying geology

The lithologies that make up the Kyrenia Range are relevant here because they provide the basis of an interpretation of the provenance of the Quaternary sediments as a whole.

The Quaternary sediments unconformably overlie a range of lithologies of Permian to Pliocene age (Fig. 2). The oldest intact sequences in the Kyrenia Range are meta-carbonate rocks of Triassic to Cretaceous age, forming the Trypa (Tripa) Group (Henson et al. 1949; Ducloz 1972 Baroz 1979; Hakyemez et al. 2000; Robertson et al. 2012). The meta-carbonate platform rocks are unconformably overlain by a range of basic/silicic volcanic rocks and pelagic carbonates, some of which are rich in diagenetically formed chert. There are also volumetrically subordinate, redeposited carbonate rocks and siliciclastic rocks, all belonging to the Lapithos (Lapta) Group (Henson et al. 1949; Ducloz 1972 Baroz 1979; Hakyemez et al. 2000; Robertson et al. 2012). The uppermost part of the Lapithos (Lapta) Group is characterised by large-scale debris-flow deposits (‘olistostromes’), which include Late Palaeozoic and Mesozoic-aged blocks of shallow-water carbonate rocks (Baroz 1979; Robertson et al. 2012). Unconformably above comes a Late Eocene to Late Miocene succession, which comprises basal non-marine to shallow-marine conglomerates, deeper-marine terrigenous-derived sandstones, marls, mudstones and, finally Messinian evaporites (Baroz 1979; Weiler 1970; Necdet and Anıl 2006; McCay and Robertson 2012; McCay et al. 2012; Robertson et al. 2014), all belonging to the Kythrea (Değirmenlik) Group. The Pliocene to Recent succession is represented by shelf-depth chalks, marls and by bioclastic calcarenites of the

Mesaoria (Mesarya) Group (Reed 1930, 1935; Henson et al. 1949; Baroz 1979; McCallum and Robertson 1995a, b). Pliocene sediments are exposed only along the southern flank of the Kyrenia Range and in the Mesaoria (Mesarya) Basin to the south. It is therefore unclear whether Pliocene sediments were ever deposited on the northern flank of the Kyrenia Range.

All of the above geological units potentially supplied detrital material to the Quaternary sediments exposed on both flanks of the Kyrenia Range. The most important supplier of terrigenous sediment was the Late Eocene–Late Miocene deep-marine gravity deposits (turbidites and debris-flow deposits). These unconformably underlie the Quaternary deposits along the northern flank of the Kyrenia Range and also along many parts of the southern flank of the range. Other important contributors are the Mesozoic meta-carbonate rocks, the Late Cretaceous–Eocene basic igneous rocks and the Late Cretaceous–Eocene pelagic carbonate rocks, some of which are chert rich. In addition, locally observed red radiolarian chert and other relatively exotic rock types (e.g. gabbro and serpentinite) are likely to have been reworked from the Early Eocene large-scale debris-flow deposits ('olistostromes'). The relative abundance of the clasts in the Quaternary deposits is influenced by the relative resistance to weathering and sedimentary transport of the different lithologies, with quartz and chert being the most resistant, as shown in studies of modern Cyprus beach deposits (Garzanti et al. 2000).

## Quaternary deposits

The Quaternary deposits in the Kyrenia Range are dominated by shallow-marine to non-marine terrace deposits. These deposits form a series of geomorphological terraces, as mapped by Ducloz (1963) and Knupp (1964) as part of a United Nations-funded project. The authors described and interpreted the Quaternary terrace deposits exposed on both sides of the Kyrenia Range, particularly the younger terraces. This work and subsequent studies also showed that both marine and the non-marine deposits outcrop widely along the northern flank of the range, whereas exclusively non-marine deposits characterise the southern flank of the range (Ducloz 1972; Baroz 1979; Dreghorn 1978; Robertson and Woodcock 1986).

The terraces were given their present names by Ducloz (1963, 1972), with modifications by Baroz (1979). More recently, Turkish names (given in parentheses), as defined by Hakyemez et al. (2000), were proposed for some but not all of the terraces. The names that we use here for the terraces, from the generally topographically highest to the generally topographically lowest are as follows: Karka, Klepini (Arapköy), Tripimeni (Tirmen), Agios Epikititos (Çatalcöy), Agios Ermolaos (Çirinevlar), Kyrenia (Girne) and Koupia terraces (Ducloz 1964; Knupp 1964; Ducloz 1972; Baroz 1979; Hakyemez et al. 2000). The preliminary mapping suggested that the youngest marine terrace, the Koupia terrace, is patchily developed along the coastline, never more than 100 m inland (Fig. 3). However, the Kyrenia (Girne) terrace is extensive along the northern coast and up to c. 2 km inland. The older marine terraces that are exposed at higher elevations further inland are not discussed here.

## Terrace deposits

Within the Kyrenia (Girne) and Koupia terrace systems, nine sections were selected, encompassing a wide range of sediment types, which are located along the coast,

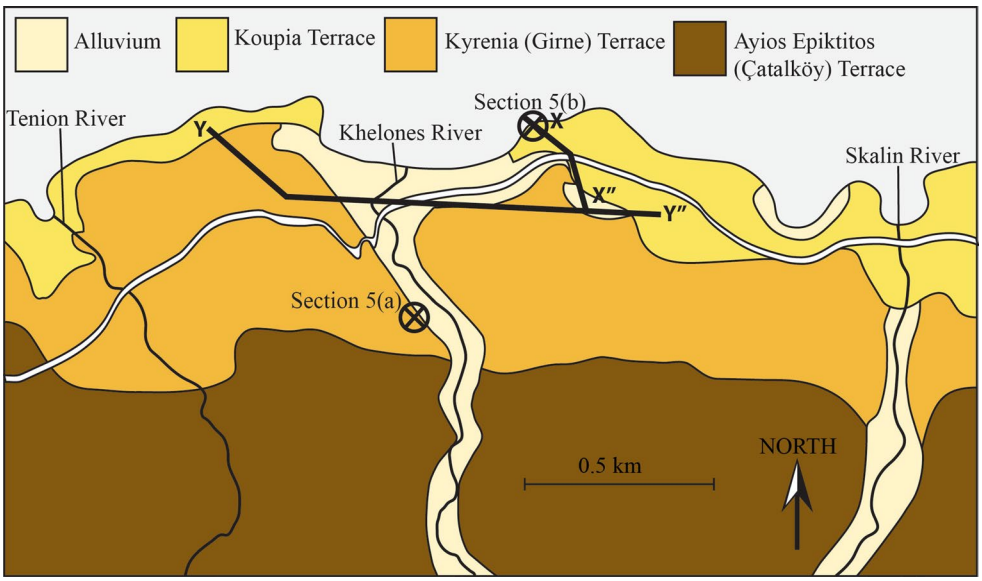


**Fig. 3** Outline geological map of the area west of Mersinlik (Flamoudi) village showing the exposed Quaternary terrace (modified from Ducloz 1963). Lines X–X″ and Y–Y″ refer to the cross sections shown in Fig. 8

some distance inland, and also on the southern flank of the Kyrenia Range. For each section, the higher-level Kyrenia (Girne) terrace deposits are described first, followed by the Koupia terrace deposits, where present, moving from west to east. Unless otherwise stated the calcarenite deposits are lithified, with a carbonate cement.

### Section 1. Vasilia (Karşıyaka) village (N35 21.465′ E033 08 360′)

In this westerly area (Fig. 2), the only exposure of the Kyrenia (Girne) terrace deposits occurs along the coastline, directly north of the highest mountain in the Kyrenia Range, Selvili Tepe (Kiparissovouno). The Kyrenia (Girne) terrace deposits are mostly comprised of calcarenite, c. 4 m thick. The basal 2 m of the section is planar-bedded, medium- to coarse-grained calcarenite. Bedding varies in thickness from 5 to 10 cm. Above there comes a 0.5-m-thick unit of bioclastic debris, with fragments of pectens, oysters, bivalves, calcareous algae and occasional *Cladocora caespitosa* (solitary coral). This, in turn, is overlain by c. 1.5 m of poorly bedded, massive calcarenite with abundant, cemented plant root traces.

The calcarenites are dominantly comprised of bioclastic grains such as bivalves, gastropods, benthic foraminifera and calcareous red algae. Volumetrically subordinate lithic fragments include chert, monocrystalline quartz, polycrystalline quartz, reworked bioclastic fragments (e.g. calcareous algae), gastropods, bivalve shell fragments and minor amounts of feldspar. The shells are calcitic with micrite-filled chambers. Pore spaces between the grains are infilled with a combination of micrite and sparite cement.

### Section 2: Alagadi beach (N35 19.978′ E033 29.535′)

Located 15 km east of Girne (Kyrenia) town, Alagadi beach (Fig. 2), provides an excellent opportunity to study the relationship between the Kyrenia (Girne) and Koupia terrace deposits. Two sections were studied: first, a deposit slightly above modern sea level and secondly a deposit c. 15 m AMSL (Figs. 4, 5). The higher deposit was previously mapped as part of the Kyrenia (Girne) terrace, whereas the lower deposit was shown as part of the Koupia terrace (Ducloz 1964). The upper deposit continues inland for c. 2 km, whereas the lower deposit is restricted to the coast.

*Lower deposit-Koupia terrace (Section 2(a))*

A 4-m-thick calcarenite sequence overlies Miocene calcareous mudstones and sandstones of the Kythrea (Değirmenlik) Group (Fig. 5). An erosional unconformity between the two units is located at ~2 m AMSL. The calcarenite contains planar-bedded sedimentary structures, especially in the lower half of the interval. In addition, rounded to sub-rounded pebbles (<0.5 mm in size) are present. Bioclastic clasts are mostly red algae, bryozoa, gastropods, benthic foraminifera and peloids. A subordinate volume of the rock is made up of monocrystalline quartz (Fig. 6a), chert (Fig. 6b), polycrystalline quartz (Fig. 6c), reworked benthic foraminifera and feldspar (Fig. 6d). In general, the calcarenite has around 30 % pore space. Cementation is mainly a microsparitic coating of grain boundaries and the partial infilling of pore space.

*Higher deposit-Kyrenia terrace (Section 2(b))*

A basal conglomerate (~30 cm thick) is rich in bioclastic debris, notably bivalves, oysters and occasional Cladocora corals. This is followed by calcarenite, c. 4 m thick, making up the remainder of the section (Fig. 4). The sediments are structureless other than for the presence of calcified root traces that are abundant in the upper part of the section.

### Section 3: Bahçeli (Kalograia) village (N35 21.076′ E033 38.378′)

This 200-m-long road section of the Kyrenia (Girne) terrace deposits is located c. 1 km east of Bahçeli (Kalograia) village (Fig. 2). The Kyrenia (Girne) terrace surface has been previously mapped in this area as continuing inland for at least 1 km (Knupp 1964). The exposed section is divisible into a lower mudstone unit, c. 4 m thick, and an upper lenticular-bedded conglomerate unit, c. 8 m thick (Fig. 7). The lower unit includes two prominent palaeosols. The upper lenticular conglomerate unit transgresses the lower unit at c. 45°, dipping eastwards. The lenticular conglomerate includes clasts of meta-carbonates, basalt, cherts and pelagic carbonates. The clasts are mostly sub-angular, and range is size from <1 to 15 cm, with a modal clast size of c. 5 cm. The individual conglomerate lenses are continuous for several metres along the length of the section and vary in thickness from 10 cm to 30 cm. Sedimentary structures are poorly developed within the lenses, with no signs of grading or sorting of the clasts.

### Section 4: Küçükerenköy village (N35 21.685′ E033 40.286′)

This coastal exposure represents the type locality of the Kyrenia (Girne) terrace (Baroz 1979). An erosional contact with underlying Miocene sandstone and mudstone is exposed at c. 6 m AMSL. The section is made up of

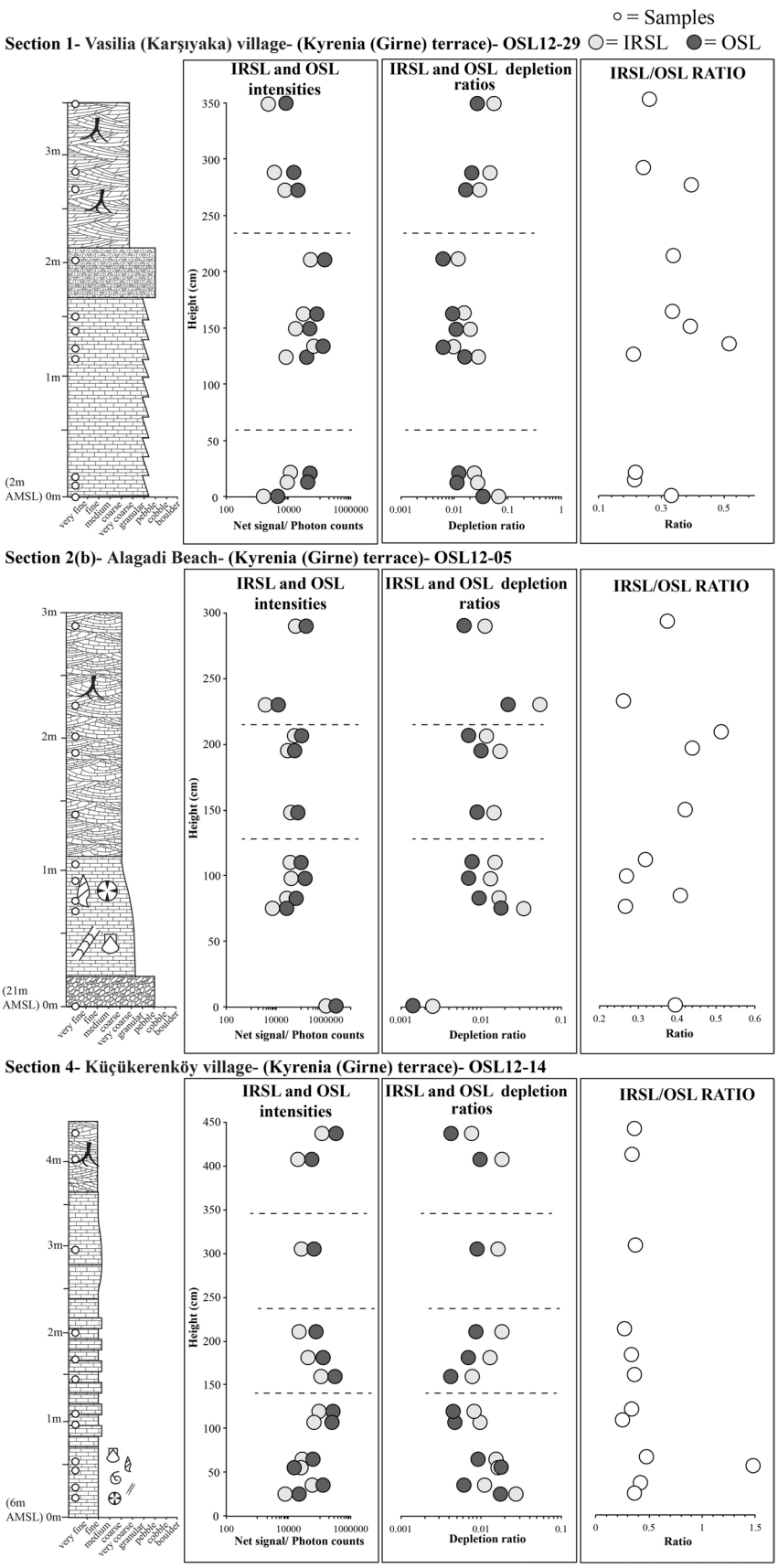


**Fig. 4** Sedimentary logs and portable luminescence profiles from calcarenite deposits of the Kyrenia (Girne) terrace on the northern flank of the Kyrenia Range. Luminescence packages are marked on the IRSL and OSL profiles by dashed horizontal lines. (Key to sedimentary logs is shown in Fig. 5)

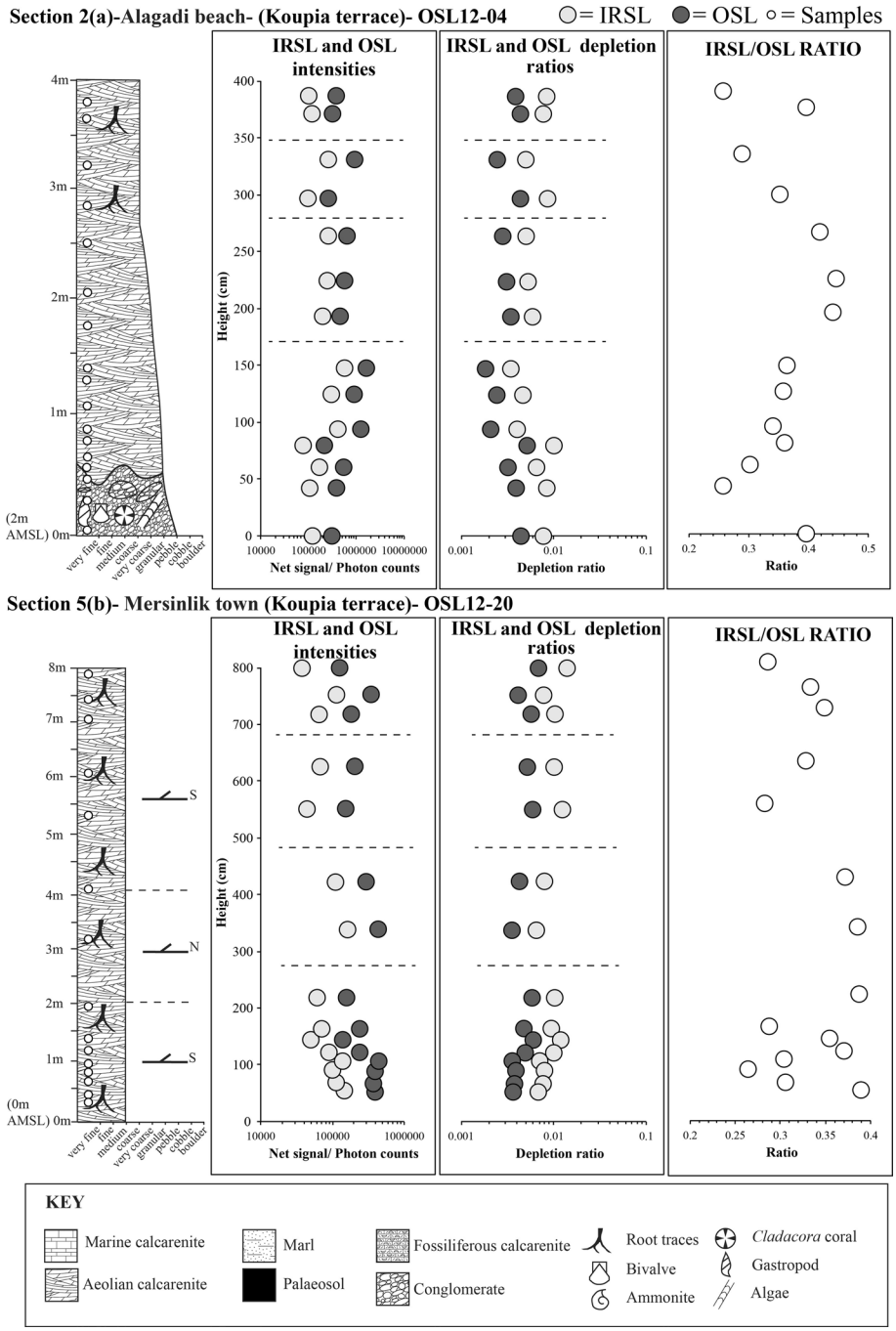


**Fig. 5** Sedimentary logs and portable luminescence profiles from calcarenite deposits of the Koupia terrace on the northern flank of the Kyrenia Range. Luminescence packages are marked on the IRSL and OSL profiles by dashed horizontal lines

fine-grained to coarse-grained calcarenites, c. 4 m thick (Fig. 4). The lower 3.5 m of this is fine- to coarse-grained calcarenite, with poorly sorted, sub-angular grains. The higher 1 m comprises well-sorted, medium-grained calcarenites, with abundant calcified root traces.

The calcarenite is dominated by bioclastic debris including red algae, bryozoa, corals, bivalves and gastropods. There are also monocrystalline quartz, chert, reworked calcarenite fragments, detrital pelagic carbonate, polycrystalline quartz, diabase/microgabbro and minor amounts of feldspar. Grains are sub-rounded to well rounded and range in size from <0.5 to 3 mm. Cementation is mainly microsparite (>80 % of the sediment volume), which is developed along the grain boundaries, whereas sparite infills pore spaces (<20 % of the sediment volume). In places, there is a bed containing bivalves (pectenids), gastropods and rare Cladocora coral fragments.

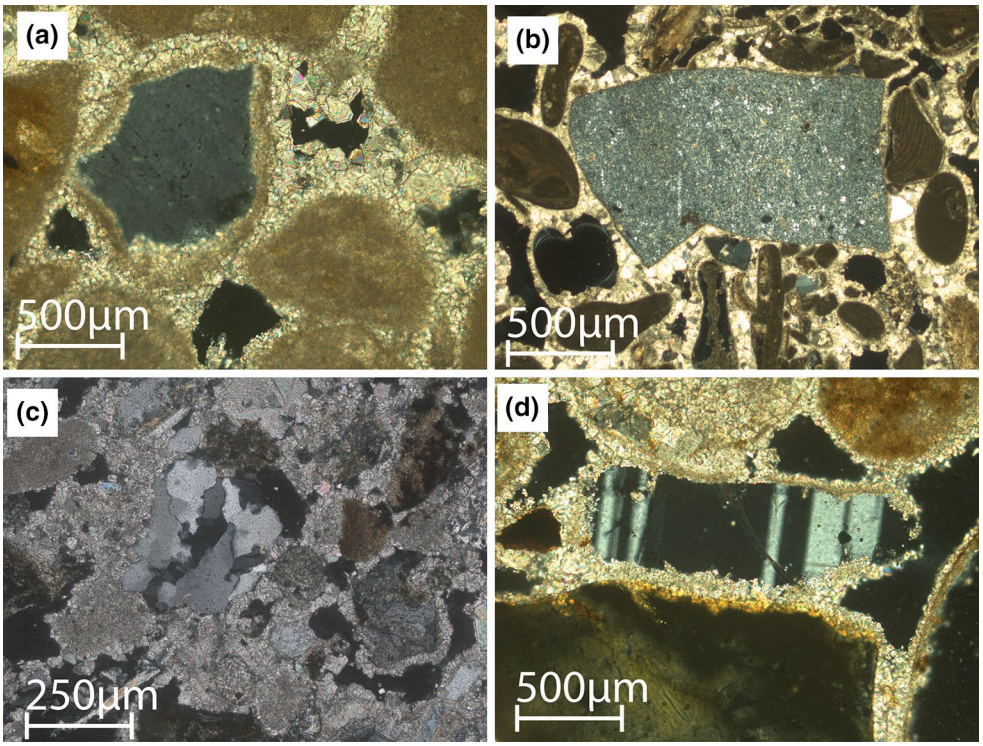


**Fig. 6** Photomicrographs of calcarenite deposits of the Kyrenia (Girne) terrace: **a** monocrystalline quartz coated in a micritic and fine sparitic cement; **b** detrital chert surrounded by reworked biogenic fragments, **c** polycrystalline quartz coated by a sparitic cement, **d** detrital plagioclase grain

**Section 5: Mersinlik village (N35 24.663′ E033 48.910′)**

This section is well exposed, both along the new main road and also along the old coastal road, c. 3 km west of Mersinlik village (Figs. 2, 3). The deposits along the main road form part of the Kyrenia (Girne) terrace system, whereas the deposits along the coastal road form part of the Koupia terrace system.

*Section 5(a)*

The Kyrenia (Girne) terrace deposit encompasses an association of lenticular conglomerates, mudstones, palaeosols and aeolianites (Fig. 7). The lower 8-m-thick, nearly 100-m-wide section is made up of lenticular conglomerate, mudstone and several palaeosols. Conglomerate lenses, c. 30 cm thick, are continuous for several metres laterally and are intercalated with fine-grained mudstone. The conglomerate is dominated by sub-angular clasts of deformed meta-carbonate rocks of the Trypa (Tripa) Group, <1 to 10 cm in size, locally showing westerly directed imbrication. Overlying the conglomerates is a well-developed dark maroon-coloured palaeosol, 1 m thick, followed by c. 3 m of aeolianite. The aeolianite exhibits a series of forests, dipping at c. 40° towards the west.

*Section 5(b)*

The Koupia terrace deposit occurs along the coast very close to modern sea level. A c. 8-m-thick sequence of crossbedded, bioclastic calcarenite is commonly exposed (Fig. 5). The grains in the calcarenite are <0.5 mm in size and sub-rounded, dominantly composed of red algae, gastropods, benthic foraminifera, peloids and bivalves. Monocrystalline quartz, polycrystalline quartz, chert, recrystallized shells and feldspar are also present. Microsparite coats all of the grains but only infills the smallest pores (c. 20 % by volume). The remaining space between the grains (c. 80 %) is filled with microsparite.

Key facies relations are shown in Fig. 8. The fluvial deposits of the Kyrenia terrace are overlain by aeolianite of the Kyrenia (Girne), representing two depositional phases within this terrace system. The cross section X–X″ shows the relationship of the aeolianites of the Kyrenia (Girne) terrace system, ~35 m AMSL to the aeolianites of the Koupia terrace system.

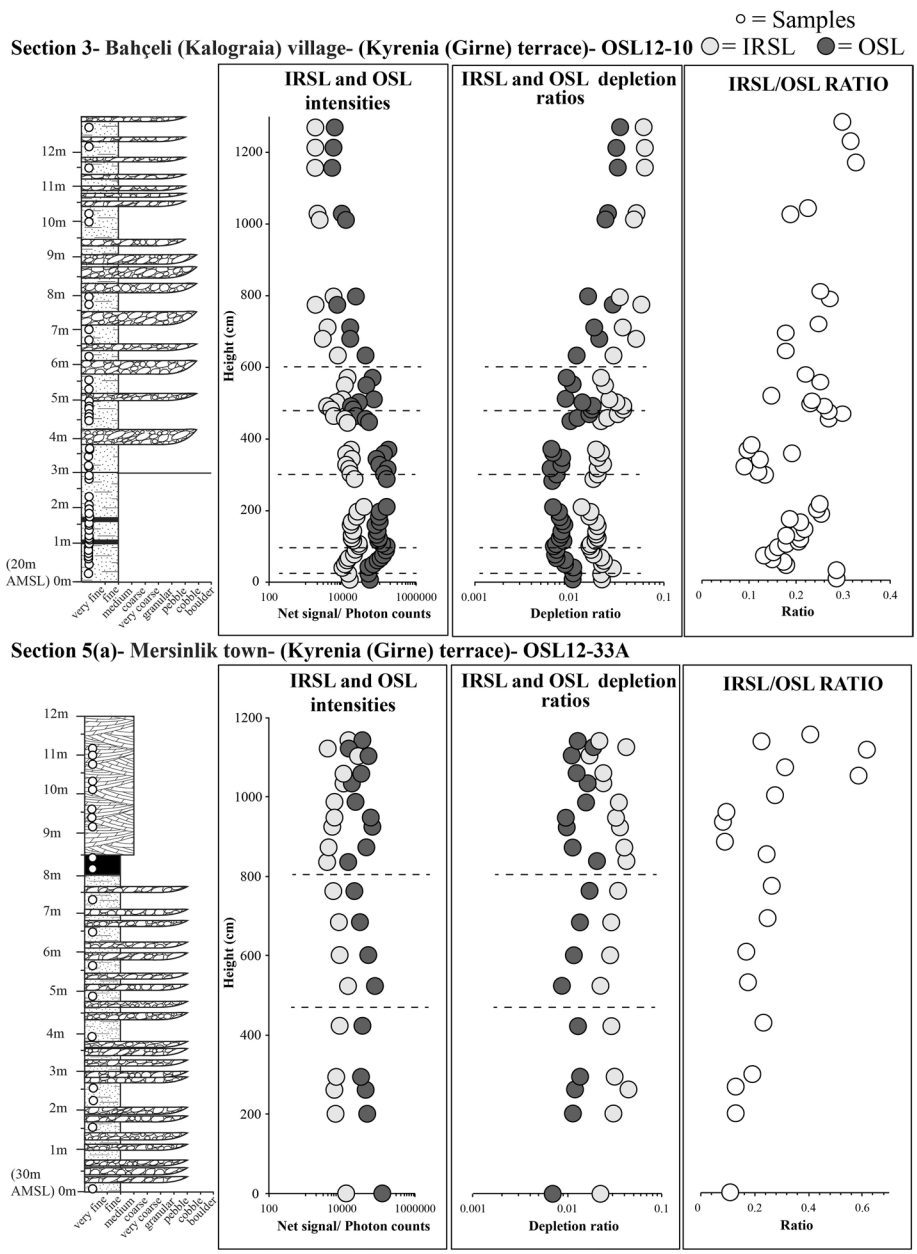


**Fig. 7** Sedimentary logs and portable luminescence profiles from mudstone, conglomerate, palaeosol and calcarenite deposits of the Kyrenia (Girne) terrace on the northern flank of the Kyrenia Range. Luminescence packages are marked on the IRSL and OSL profiles by dashed horizontal lines. (key to sedimentary logs shown in Fig. 5)

### Section 6: Kalkanlı (Kapouti) village (N35 19.012′ E033 03.016′)

The mapping by Ducloz (1963) and by Knupp (1964) was restricted to the central Kyrenia Range. The Quaternary terrace deposits of the western, eastern and southern flanks of the range have not previously been defined in terms of relative ages. However, two terrace deposits from the southern side of the range are used here to document non-marine depositional environments during the Quaternary.

This first section of non-marine deposits is from a large gully to the south-west of the Kyrenia Range (Fig. 2). These sediments are shown on the Cyprus Geological Survey Map (Constantinou 1995) as Quaternary, but were not assigned a specific terrace name. Specifically, the section is near Kalkanlı (Kapouti), within an east–west-trending gully to the north of the village of this name. The deposits are mainly lenticular, clast-supported conglomerates, interbedded with mudstones (Fig. 9). The clasts are 1–10 cm in size, sub-angular, poorly sorted and dominated by meta-carbonate of the Trypa (Tripa) Group. The matrix is fine-grained, maroon-coloured mud, forming a 1-m-thick layer between lenticular conglomerates (Fig. 9).

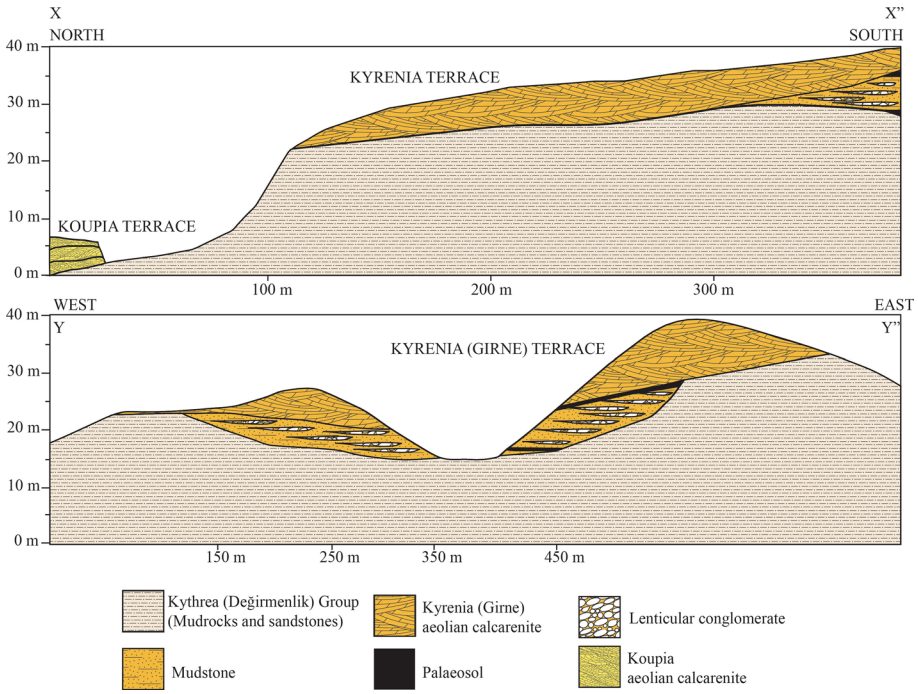


**Fig. 8** N–S and E–W cross sections through the Kyrenia (Girne) and Koupia terrace deposits near Mersinlik (Flamoudi) (see Fig. 2 for section locations)

**Section 7: Nergisli (Genagra) village (N35 12.613′ E033 42.125′)**

The second, south-of-the-range, comparative section is near Nergisli (Genagra), a village north-west of Gazimagusa (Famagusta) (Fig. 2). This deposit is again outside the area mapped by Ducloz (1963) and by Knupp (1964); it was inferred to be a Quaternary terrace deposit, but no specific terrace name was given. A small quarry near the north-western edge of the village exposes a mixture of medium-grained sand and lenticular, clast-supported conglomerate (Fig. 9). The conglomerate clasts are subrounded and range from 1 to 10 cm in size. The clasts are mostly sandstone, pelagic carbonate, chert, basalt, diabase and microgabbro. Clast imbrication indicates palaeoflow towards the south. The grains within the interbedded sands are mostly angular.

## Calcarenite composition

Calcarenite comprises a significant portion of both the Kyrenia (Girne) and Koupia terraces and accumulated in both marine and aeolian depositional environments based on their sedimentary features (see Frébourg et al. 2008). The calcarenite grains have varying proportions of carbonate and siliciclastic grains, influenced by the depositional environment and sediment provenance. The relative amount of quartz and feldspar, and therefore the depositional setting and provenance, is significant for the luminescence analysis. Point count data were collected from five marine and aeolian calcarenite deposits from both the Kyrenia (Girne) and Koupia terraces. Four hundred grains were counted per sample in the following categories: monocrystalline quartz, polycrystalline quartz, feldspar, chert, volcanic grains, metamorphic grains, sedimentary grains, calcareous red algae, bivalve fragments, calcareous algae, benthic foraminifera, echinoderm fragments, gastropods, bryozoa and ostracods (Fig. 10).

Monocrystalline quartz within the Kyrenia (Girne) terrace marine calcarenites makes up <5 %, whereas in the Kyrenia (Girne) and Koupia terrace aeolian calcarenites this ranges from 15 to 30 %. Polycrystalline quartz in both Kyrenia (Girne) and Koupia terrace marine and aeolian calcarenites is <15 %. The feldspar content in all of the calcarenite deposits is <5 %. The reworked metamorphic grains, which include metamorphic quartz, range from <5 to 15 %. Reworked sedimentary grains, which commonly include monocrystalline quartz, range from 5 % to nearly 45 %. The carbonate grains are dominantly reworked calcareous red algae with a minor component of benthic foraminifera and echinoderm fragments (with algal encrustations).

## Luminescence screening measurements

### Basic principles of luminescence

OSL dating is widely used to determine the depositional age of sediment in a diverse range of environments (see Rhodes 2011). The underlying principle is that naturally

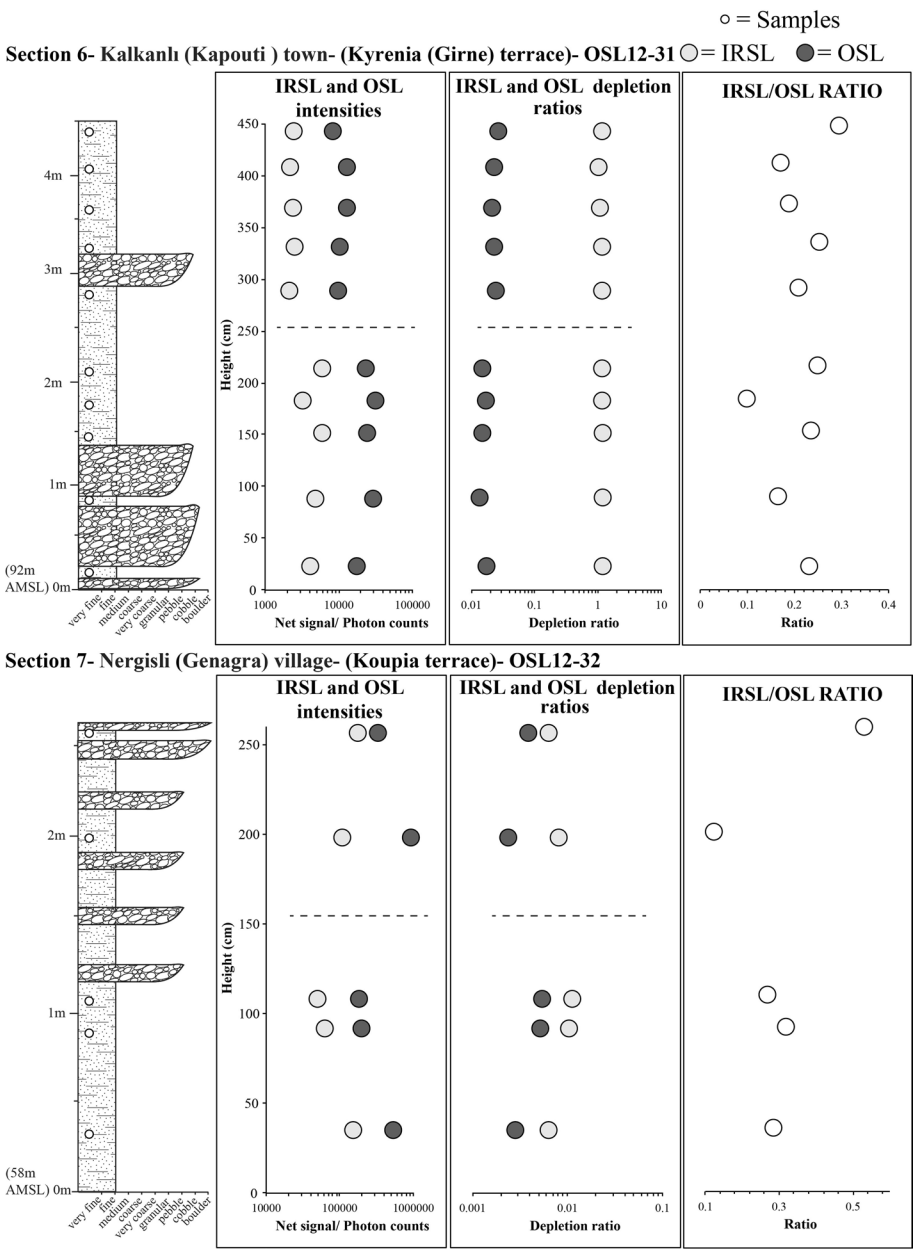


**Fig. 9** Sedimentary logs and portable luminescence profiles from mudstone and lenticular conglomerate deposits of the Kyrenia (Girne) and Koupia terraces on the southern side of the Kyrenia Range. Luminescence packages are marked on the IRSL and OSL profiles by *dashed horizontal lines*. (key to sedimentary logs shown in Fig. 5)

occurring minerals can store energy through crystal defects trapping charge in response to ionising radiation from the natural environment. Stimulated luminescence measurements are used to register the extent of trapping and, in combination with known laboratory radiation exposure, to determine the radiation dose received since an earlier zeroing event (caused by surface exposure in the past). A luminescence age (ka) is the quotient of the stored dose (Gy) and the environmental dose rate (mGy $a^{-1}$). Where sediments are well zeroed, for example, by multiple cycles of exposure to daylight prior to final deposition, the method can give highly accurate and precise ages for events ranging from recent time back to several hundred thousand years (Lian and Roberts 2006). For luminescence dating, it is important to understand that the degree of zeroing or optical bleaching is dependent on the mineral type/composition, depositional mechanism and environmental setting. The term 'bleaching' refers to the removal of trapped charge populations from a sample (Rhodes 2011). The term 'luminescence residual' refers to the geological and/or environmental luminescence signals (previous to growth of an in situ luminescence signal during a depositional cycle) that remain following a zeroing event. A number of OSL screening methods have been developed to provide insights into the luminescence properties of sediment and to interpret the depositional mechanisms and zeroing process. These range from instrumentation developments, such as the portable OSL equipment developed at the Scottish

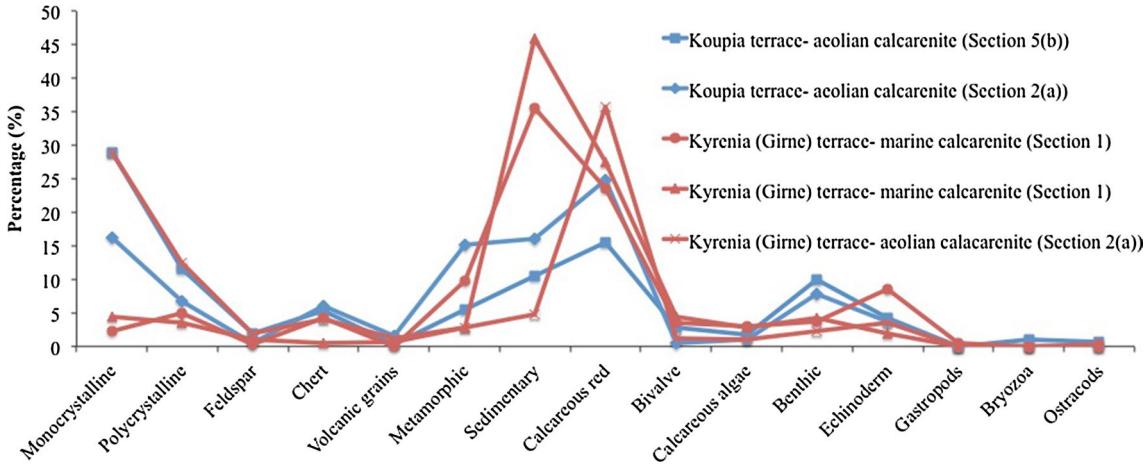


**Fig. 10** Point count data from marine and aeolian calcarenite deposits along the northern coastline of Cyprus from the Kyrenia (Girne) and Koupia terraces

Universities Environmental Research Centre (SUERC), and methodological developments such as laboratory profiling (Sanderson et al. 2001, 2003; Burbidge et al. 2007), range-finder ages (Roberts et al. 2009; Durcan et al. 2010) and standardized growth curves (e.g. Roberts and Duller 2004). Here, we use a combination of field-based luminescence profiling, in situ gamma spectrometry and sedimentological characteristics to evaluate the luminescence properties of the Kyrenia (Girne) and Koupia terrace deposits and establish a correlation of the two terrace systems on both flanks of the range.

## Luminescence analyses

Luminescence profiling was conducted in the field and subsequently in the laboratory (for bleaching experiments), using the SUERC portable OSL reader. Full details of the reader are given in Sanderson and Murphy (2010). In brief, the OSL reader consists of a sample chamber, a detector head including an ETL photodetector module with a 25-mm bi-alkali photomultiplier. Stimulation is delivered through either blue LEDs emitting 470 nm (OSL) or infrared LEDs emitting 880 nm (IRSL). The blue diodes are outfitted with GG420 long-pass filters, whereas the IR diode ports are outfitted with RG780 long-pass filters. Both signals pass through UG11 filters, and detection is attained by a 24-bit photon counter, which is set for continuous wave counting (see Sanderson and Murphy 2010).

The measurement cycle used here utilised an interleaved sequence of system dark count (background), IRSL and OSL, similar to that described by Sanderson and Murphy (2010). This enabled net IRSL and OSL signal intensities, depletion indices and the IRSL:OSL ratios to be calculated for each sample. The interpretation of the OSL signal intensities, their depletion indices and the IRSL:OSL ratio have been discussed in a number of recent publications (Sanderson and Murphy 2010; Muñoz-Salinas et al. 2011; Kinnaird et al. 2012; Munyikwa et al. 2012). The IRSL and OSL intensities may act as age proxies in well-bleached sedimentary units, assuming common sensitivities and dose rates. Luminescence sensitivity is a measure of signal intensity per unit of absorbed radiation dose. Whereas OSL intensity is a function of the amount of radiation exposure to the minerals since burial, sensitivity relates to the efficiency with which the absorbed radiation is transmitted as luminescence. Any discontinuities or 'inversions' in the OSL signal intensity profiles may reflect differences in the initial sedimentary characteristics or depositional circumstances. If mineralogical composition, grain size or diagenesis varies throughout a section, then signal intensities will also reflect such changes. The depletion index, which represents the proportion of signal released in the first half of a stimulation cycle relative to the second half, is an indicator of sample transparency, coupled with information about whether a sample contains an inherited or signal cycle signal. Higher depletion indices would indicate better-bleached material. The IRSL:OSL ratio is potentially sensitive to mineralogical input changes, potentially reflecting quartz/feldspar relative contents, and the weathering history of the sediment. These proxies are used here in conjunction with the sedimentological observations to provide an initial interpretation of the luminescence properties of individual samples, with a view to generating 'luminescence stratigraphies'. The aim is to obtain information on individual sample luminescence characteristics and sample-to-sample variations between, and also within, the terrace deposits. A further objective of the luminescence investigation is to

explore the variation in the residual luminescence signals of the near-shore versus the terrestrial sediments of the two terrace systems and to interpret the processes of sediment bleaching in contrasting depositional environments with different sediment sources and transport histories.

The sensitivities of the quartz and the polymineral signals to bleaching were also investigated. Samples were selected from the Kyrenia (Girne) and Koupia terrace deposits at Alagadi beach (Section 2, OSL12-04 and 05) and from the Koupia terrace deposits at Mersinlik (Section 5, OSL12-20). Representative samples were exposed in natural daylight for a number of different time durations (between 1 and 90 min), prior to recording the net IRSL and OSL signal intensities, as outlined above.

## Sampling

A set of 107 samples was collected through the nine sections described above (see Fig. 2). The sample set from the Kyrenia (Girne) terrace system includes marine and aeolian deposits (3 localities) and also fluvial deposits (3 localities). In contrast, the Koupia terrace system sample set comprises two marine/aeolian deposits (2 localities) and one fluvial deposit (1 locality). Samples were collected every 10 cm to 1 m through each stratigraphic section.

At each selected section, the sediment profile was first cut back by at least 10 cm, to remove superficial material which had been light-exposed, subject to weathering or near-surface drying. All of the samples were collected under light-safe conditions using opaque (black) covers. The samples were either collected by driving 20 mm × 50 mm diameter copper tubes into the cleaned section or by using a pick to remove the sediment from the section directly into 50-mm-sized petri dishes for measurement in the portable reader. The marine and aeolian calcarenite deposits, although relatively young, were semilithified and, therefore, only required use of a toothpick to granulate the samples into a petri dish in the field. In situ field gamma spectrometer (FGS) measurements were taken from a number of representative lithologies in each terrace. FGS measurements were made using a health physics instrument rainbow multichannel analyser with a 2 × 2″ NaI probe.

## Results

Net IRSL and OSL signal intensities, their depletion indices and the IRSL:OSL ratios were calculated (after background subtraction) for all samples. All of the samples yielded measureable luminescence signals that exceeded system backgrounds. The data were then plotted relative to height in their respective sedimentary sequence, as shown in Figs. 4, 5, 7 and 9 (see also Tables 1, 2, 3, 4, 5). All of the samples exhibited brighter OSL than IRSL intensities. The OSL and IRSL intensities exhibit a strong correlation, i.e. for the samples that emitted a relatively dim blue signal the corresponding red signal was also dim (Fig. 11). The mineral assemblage in both the Koupia and Kyrenia deposits is dominated by quartz (from a variety of sources), carbonate bioclasts, but only minor proportions of feldspar. Point count data show that both the aeolian and the marine calcarenites are rich in quartz grains but contain only a minor feldspar component. The available compositional data suggest that the luminescence signals were derived from a similar assemblage of minerals in similar proportions in all of the samples studied.

The luminescence proxy variables measured by the portable unit are influenced by: (1) sediment grain size and colour, (2) the total radiation dose that the sediment has been exposed to during burial, (3) the sensitivity (brightness) of the luminescence signal of the minerals present, (4) the degree of signal resetting through sunlight exposure that the sediment has experienced prior to deposition and (5) the post-depositional age of the sediment. A number of these variables can be constrained by sedimentological observations, as summarised above. Local variations in grain characteristics (variable (1)) were taken into consideration when interpreting signal intensities; however, no correlation was noted between grain characteristics and signal intensities.

Variable (2) was accounted for by in situ gamma dose rate measurements that were made at a number of localities, encompassing both marine and fluvial deposits, and from terraces on either side of the range (Table 5). Within the Koupia terrace, the measured in situ gamma dose rates varied between 0.6 and 0.9 mGy $a^{-1}$. In contrast, within the Kyrenia (Girne) terrace sections, these values range between 0.3 and 1.8 mGy $a^{-1}$. Some lithological control was noted. For the calcarenite deposits (Sections 1 and 5(b)), the gamma dose rate recorded varied between 0.5 and 1.0 mGy $a^{-1}$. For the mudstones and the palaeosols, gamma dose rates ranged from 0.5 to 1.8 mGy $a^{-1}$. When comparing signal intensities in the Kyrenia (Girne) and Koupia terrace deposits in adjacent areas, only sediments of similar composition were utilised thereby taking account of local variations in environmental dose rates.

For variable (3), any difference in the mineral composition is likely to have an important influence on the sensitivity (brightness) of the luminescence signal. This sensitivity is likely to fluctuate, given the varied provenance of the Kyrenia Range sediments and the potential for multiple sediment transport pathways prior to deposition. Despite this, the variations in signal intensities are low and the IRSL:OSL ratios are similar for samples from within the individual sections of both the Kyrenia (Girne) and Koupia depositional systems; these measurements were again similar for each of the two terrace systems.

**Table 1** IRSL, OSL and depletion data, with associated errors, for the Kyrenia (Girne) terrace marine and aeolian calcarenite deposits on the northern coastline of Cyprus

| Locality | GPS | Lithology | Height (cm) | IRSL | Error | IRSL depletion | Error | OSL | Error | OSL depletion | Error | IRSL/OSL ratio | Error |
|---|---|---|---|---|---|---|---|---|---|---|---|---|---|
| Section 1 Karşiyaka (Vasilia) (OSL 12-29) Kyrenia (Girne) terrace | N35 21.627′ E033 08.277′ | Calcarenite | 0.0 | 1487 | 48 | 1.01 | 0.07 | 4492 | 73 | 1.06 | 0.03 | 0.331 | 0.012 |
| | | Calcarenite | 13.1 | 9267 | 100 | 1.20 | 0.03 | 42,527 | 208 | 1.16 | 0.01 | 0.218 | 0.003 |
| | | Calcarenite | 20.6 | 10,950 | 108 | 1.22 | 0.02 | 50,278 | 225 | 1.36 | 0.01 | 0.218 | 0.002 |
| | | Calcarenite | 124.1 | 8271 | 96 | 1.19 | 0.03 | 39,125 | 200 | 1.53 | 0.02 | 0.211 | 0.003 |
| | | Calcarenite | 133.2 | 65,482 | 258 | 1.25 | 0.01 | 126,652 | 356 | 1.10 | 0.01 | 0.517 | 0.003 |
| | | Calcarenite | 148.5 | 17,999 | 137 | 1.25 | 0.02 | 45,862 | 216 | 1.15 | 0.01 | 0.392 | 0.004 |
| | | Calcarenite | 162.1 | 28,537 | 171 | 1.26 | 0.02 | 85,118 | 293 | 1.35 | 0.01 | 0.335 | 0.002 |
| | | Calcarenite | 210.7 | 51,758 | 230 | 1.29 | 0.01 | 153,537 | 393 | 1.21 | 0.01 | 0.337 | 0.002 |
| | | Calcarenite | 273.0 | 7983 | 93 | 1.25 | 0.03 | 20,138 | 144 | 1.17 | 0.02 | 0.396 | 0.005 |
| | | Calcarenite | 288.0 | 3519 | 66 | 1.21 | 0.05 | 14,499 | 124 | 1.20 | 0.02 | 0.243 | 0.005 |
| | | Calcarenite | 349.0 | 2203 | 54 | 1.13 | 0.06 | 8433 | 96 | 1.18 | 0.03 | 0.261 | 0.007 |
| Section 2(b) Alagadi beach OSL 12-05 Kyrenia (Girne) | N35 20.138′E033 29.342′ | Calcarenite | 1.0 | 1,041,579 | 1023 | 1.26 | 0.00 | 2,633,073 | 1624 | 1.15 | 0.001 | 0.396 | 0.000 |
| | | Calcarenite | 75.4 | 6853 | 103 | 1.13 | 0.03 | 25,565 | 171 | 1.31 | 0.02 | 0.268 | 0.004 |
| | | Calcarenite | 83.2 | 25,558 | 171 | 1.24 | 0.02 | 62,597 | 258 | 1.15 | 0.01 | 0.408 | 0.003 |
| | | Calcarenite | 98.2 | 38,682 | 206 | 1.24 | 0.01 | 143,290 | 383 | 1.27 | 0.01 | 0.270 | 0.002 |
| | | Calcarenite | 110.4 | 33,444 | 194 | 1.28 | 0.01 | 105,063 | 330 | 1.23 | 0.01 | 0.318 | 0.002 |
| | | Calcarenite | 148.1 | 32,205 | 190 | 1.21 | 0.01 | 76,617 | 284 | 1.19 | 0.01 | 0.420 | 0.003 |
| | | Calcarenite | 194.8 | 26,588 | 174 | 1.30 | 0.02 | 60,550 | 253 | 1.18 | 0.01 | 0.439 | 0.003 |
| | | Calcarenite | 206.6 | 54,027 | 240 | 1.27 | 0.01 | 105,300 | 330 | 1.12 | 0.01 | 0.513 | 0.003 |
| | | Calcarenite | 230.0 | 3570 | 86 | 1.12 | 0.05 | 13,574 | 132 | | 0.02 | 0.263 | 0.007 |
| | | Calcarenite | 289.8 | 58,902 | 250 | 1.30 | 0.01 | 156,860 | 401 | 1.19 | 0.01 | 0.376 | 0.002 |
| Section 4 Küçükerenköy OSL12-14 Kyrenia (Girne) terrace | N35 21.849′E033 40.160′ | Calcarenite | 25.1 | 8009 | 91 | 1.18 | 0.03 | 21,835 | 149 | 1.25 | 0.02 | 0.367 | 0.005 |
| | | Calcarenite | 36.3 | 55,561 | 237 | 1.26 | 0.01 | 131,705 | 364 | 1.10 | 0.01 | 0.422 | 0.002 |
| | | Calcarenite | 55.7 | 23,464 | 154 | 1.22 | 0.02 | 15,904 | 128 | 1.08 | 0.02 | 1.475 | 0.015 |
| | | Calcarenite | 65.8 | 27,014 | 166 | 1.23 | 0.02 | 57,270 | 240 | 1.10 | 0.01 | 0.472 | 0.004 |
| | | Calcarenite | 107.0 | 64,206 | 256 | 1.22 | 0.01 | 245,219 | 495 | 1.16 | 0.005 | 0.262 | 0.001 |
| | | Calcarenite | 119.5 | 95,386 | 310 | 1.26 | 0.01 | 276,970 | 527 | 1.17 | 0.004 | 0.344 | 0.001 |
| | | Calcarenite | 159.3 | 112,643 | 338 | 1.30 | 0.01 | 310,654 | 559 | 1.17 | 0.004 | 0.363 | 0.001 |
| | | Calcarenite | 181.7 | 42,577 | 208 | 1.30 | 0.01 | 125,836 | 355 | 1.21 | 0.01 | 0.338 | 0.002 |
| | | Calcarenite | 210.9 | 21,487 | 148 | 1.30 | 0.02 | 78,476 | 281 | 1.22 | 0.01 | 0.274 | 0.002 |
| | | Calcarenite | 305.4 | 24,936 | 159 | 1.26 | 0.02 | 66,092 | 258 | 1.14 | 0.01 | 0.377 | 0.003 |
| | | Calcarenite | 407.2 | 20,142 | 144 | 1.27 | 0.02 | 58,596 | 243 | 1.15 | 0.01 | 0.344 | 0.003 |
| | | Calcarenite | 437.0 | 121,763 | 349 | 1.31 | 0.01 | 333,976 | 578 | 1.21 | 0.004 | 0.365 | 0.001 |

**Table 2** IRSL, OSL and depletion data, with associated errors, for the Koupia terrace marine and aeolian calcarenite deposits on the northern coastline of Cyprus

| Locality | GPS | Lithology | Height (cm) | IRSL | Error | IRSL depletion | Error | OSL | Error | OSL depletion | Error | IRSL/OSL ratio | Error |
|---|---|---|---|---|---|---|---|---|---|---|---|---|---|
| Section 2(a) Alagadi beach OSL 12-04 Koupia terrace | N35 20.138′ E033 29.342′ | Calcarenite | 0.0 | 119,104 | 360 | 1.27 | 0.01 | 301,546 | 558 | 1.17 | 0.004 | 0.395 | 0.001 |
| | | Calcarenite | 42.1 | 100,387 | 332 | 1.26 | 0.01 | 389,017 | 631 | 1.20 | 0.004 | 0.258 | 0.001 |
| | | Calcarenite | 60.2 | 164,232 | 418 | 1.26 | 0.01 | 545,472 | 746 | 1.17 | 0.003 | 0.301 | 0.001 |
| | | Calcarenite | 79.3 | 75,540 | 292 | 1.27 | 0.01 | 210,654 | 470 | 1.15 | 0.005 | 0.359 | 0.002 |
| | | Calcarenite | 93.8 | 414,537 | 652 | 1.26 | 0.00 | 1,215820 | 1107 | 1.13 | 0.002 | 0.341 | 0.001 |
| | | Calcarenite | 124.2 | 306,639 | 563 | 1.25 | 0.00 | 858,179 | 932 | 1.13 | 0.002 | 0.357 | 0.001 |
| | | Calcarenite | 147.0 | 571,434 | 763 | 1.28 | 0.00 | 1,576,657 | 1260 | 1.16 | 0.002 | 0.362 | 0.001 |
| | | Calcarenite | 192.9 | 195,403 | 453 | 1.28 | 0.01 | 443,644 | 673 | 1.13 | 0.003 | 0.440 | 0.001 |
| | | Calcarenite | 223.7 | 244,420 | 504 | 1.27 | 0.01 | 548,902 | 748 | 1.12 | 0.003 | 0.445 | 0.001 |
| | | Calcarenite | 263.3 | 265,151 | 525 | 1.27 | 0.01 | 631,718 | 801 | 1.12 | 0.003 | 0.420 | 0.001 |
| | | Calcarenite | 296.4 | 93,419 | 321 | 1.25 | 0.01 | 265,347 | 525 | 1.11 | 0.004 | 0.352 | 0.001 |
| | | Calcarenite | 331.1 | 260,111 | 520 | 1.25 | 0.01 | 903,712 | 957 | 1.15 | 0.002 | 0.288 | 0.001 |
| | | Calcarenite | 371.0 | 119,104 | 360 | 1.27 | 0.01 | 301,546 | 558 | 1.17 | 0.004 | 0.395 | 0.001 |
| | | Calcarenite | 386.5 | 100,387 | 332 | 1.26 | 0.01 | 389,017 | 631 | 1.20 | 0.004 | 0.258 | 0.001 |
| Section 5(b) Mersinlik OSL12-20 Koupia terrace | N35 24.761′ E033 48.659′ | Calcarenite | 54.0 | 148,668 | 387 | 1.29 | 0.01 | 381,496 | 619 | 1.14 | 0.004 | 0.390 | 0.001 |
| | | Calcarenite | 67.0 | 113,826 | 339 | 1.27 | 0.01 | 371,789 | 611 | 1.15 | 0.004 | 0.306 | 0.001 |
| | | Calcarenite | 90.0 | 103,119 | 322 | 1.27 | 0.01 | 391,614 | 627 | 1.21 | 0.004 | 0.263 | 0.001 |
| | | Calcarenite | 107.0 | 133,994 | 368 | 1.26 | 0.01 | 439,466 | 664 | 1.18 | 0.004 | 0.305 | 0.001 |
| | | Calcarenite | 122.0 | 86,498 | 296 | 1.43 | 0.01 | 233,570 | 485 | 1.18 | 0.005 | 0.370 | 0.001 |
| | | Calcarenite | 144.0 | 49,702 | 226 | 1.28 | 0.01 | 140,142 | 376 | 1.14 | 0.006 | 0.355 | 0.002 |
| | | Calcarenite | 164.0 | 70,849 | 268 | 1.24 | 0.01 | 246,359 | 498 | 1.18 | 0.005 | 0.288 | 0.001 |
| | | Calcarenite | 219.0 | 61,082 | 249 | 1.26 | 0.01 | 157,597 | 399 | 1.15 | 0.006 | 0.388 | 0.002 |
| | | Calcarenite | 338.0 | 163,614 | 406 | 1.30 | 0.01 | 423,453 | 652 | 1.16 | 0.004 | 0.386 | 0.001 |
| | | Calcarenite | 423.0 | 109,640 | 333 | 1.29 | 0.01 | 295214 | 544 | 1.15 | 0.004 | 0.371 | 0.001 |
| | | Calcarenite | 551.0 | 43,750 | 212 | 1.28 | 0.01 | 154,710 | 395 | 1.17 | 0.006 | 0.283 | 0.002 |
| | | Calcarenite | 625.3 | 66,895 | 261 | 1.25 | 0.01 | 203,815 | 453 | 1.15 | 0.005 | 0.328 | 0.001 |
| | | Calcarenite | 718.5 | 64,410 | 256 | 1.30 | 0.01 | 184,636 | 431 | 1.20 | 0.006 | 0.349 | 0.002 |
| | | Calcarenite | 753.4 | 113,757 | 339 | 1.29 | 0.01 | 341,088 | 585 | 1.19 | 0.004 | 0.334 | 0.001 |
| | | Calcarenite | 798.2 | 36,957 | 196 | 1.30 | 0.01 | 128,795 | 360 | 1.22 | 0.007 | 0.287 | 0.002 |

**Table 3** IRSL, OSL and depletion data, with associated errors, for the Kyrenia (Girne) terrace fluvial deposits on the northern coastline of Cyprus

| Locality | GPS | Lithology | Height (cm) | IRSL | Error | IRSL depletion | Error | OSL | Error | OSL depletion | Error | IRSL/OSL ratio | Error |
|---|---|---|---|---|---|---|---|---|---|---|---|---|---|
| Section 3 Bahçeli (Kalograi) OSL12-10 Kyrenia (Girne) terrace | N35 21.222′ E033 38.141′ | Mudstone | 10.0 | 15,601 | 137 | 1.24 | 0.02 | 54,901 | 241 | 1.22 | 0.01 | 0.284 | 0.003 |
| | | Mudstone | 27.0 | 14,262 | 124 | 1.23 | 0.02 | 49,935 | 226 | 1.19 | 0.01 | 0.286 | 0.003 |
| | | Mudstone | 41.0 | 9275 | 102 | 1.28 | 0.03 | 52,271 | 231 | 1,22 | 0.01 | 0.177 | 0.002 |
| | | Mudstone | 53.0 | 12,154 | 115 | 1.21 | 0.02 | 70,861 | 268 | 1.19 | 0.01 | 0.172 | 0.002 |
| | | Mudstone | 60.0 | 12,528 | 117 | 1.26 | 0.02 | 85,140 | 293 | 1.27 | 0.01 | 0.147 | 0.001 |
| | | Mudstone | 69.0 | 14,575 | 125 | 1.23 | 0.02 | 110,701 | 334 | 1.23 | 0.01 | 0.132 | 0.001 |
| | | Mudstone | 79.0 | 19,946 | 145 | 1.25 | 0.02 | 130,504 | 363 | 1.25 | 0.01 | 0.153 | 0.001 |
| | | Palaeosol | 90.0 | 22,404 | 153 | 1.26 | 0.02 | 135283 | 369 | 1.31 | 0.01 | 0.166 | 0.001 |
| | | Palaeosol | 101.0 | 26,690 | 166 | 1.27 | 0.02 | 147,932 | | 1.34 | 0.01 | 0.180 | 0.001 |
| | | Palaeosol | 109.0 | 24,334 | 159 | 1.29 | 0.02 | 119,865 | 348 | 1.26 | 0.01 | 0.203 | 0.001 |
| | | Mudstone | 117.0 | 18,405 | 140 | 1.27 | 0.02 | 88,742 | 300 | 1.26 | 0.01 | 0.207 | 0.002 |
| | | Mudstone | 125.0 | 17,260 | 134 | 1.28 | 0.02 | 95,482 | 310 | 1.26 | 0.01 | 0.181 | 0.002 |
| | | Mudstone | 134.0 | 17,294 | 133 | 1.23 | 0.02 | 83,366 | 290 | 1.21 | 0.01 | 0.207 | 0.002 |
| | | Mudstone | 144.0 | 18,241 | 137 | 1.27 | 0.02 | 84,465 | 292 | 1.19 | 0.01 | 0.216 | 0.002 |
| | | Mudstone | 159.6 | 15,927 | 128 | 1.22 | 0.02 | 77,069 | 279 | 1.23 | 0.01 | 0.207 | 0.002 |
| | | Mudstone | 170.8 | 17,238 | | 1.23 | 0.02 | 91,241 | 303 | 1.25 | 0.01 | 0.189 | 0.002 |
| | | Palaeosol | 181.9 | 23,841 | 156 | 1.24 | 0.02 | 94,786 | 309 | 1.19 | 0.01 | 0.252 | 0.002 |
| | | Palaeosol | 196.1 | 25,294 | 161 | 1.29 | 0.02 | 102,775 | 321 | 1.23 | 0.01 | 0.246 | 0.002 |
| | | Palaeosol | 209.3 | 38,557 | 198 | 1.29 | 0.01 | 153,212 | 392 | 1.29 | 0.01 | 0.252 | 0.001 |
| | | Mudstone | 288.2 | 19,396 | 142 | 1.22 | 0.02 | 144,609 | 381 | 1.21 | 0.01 | 0.134 | 0.001 |
| | | Mudstone | 300.6 | 16,043 | 129 | 1.24 | 0.02 | 133,548 | 366 | 1.31 | 0.01 | 0.120 | 0.001 |
| | | Mudstone | 316.0 | 14,323 | 122 | 1.17 | 0.02 | 163,732 | 405 | 1.27 | 0.01 | 0.087 | 0.001 |
| | | Mudstone | 332.0 | 11,985 | 113 | 1.20 | 0.02 | 9,672 S | 312 | 1.27 | 0.01 | 0.124 | 0.001 |
| | | Mudstone | 348.2 | 16,379 | 130 | 1.27 | 0.02 | 85,641 | 294 | 1.23 | 0.01 | 0.191 | 0,002 |
| | | Mudstone | 359.4 | 12,989 | 116 | 1.21 | 0.02 | 136,538 | 370 | 1.22 | 0.01 | 0.095 | 0.001 |
| | | Mudstone | 371.5 | 17842 | 135 | 1.27 | 0.02 | 168,540 | 411 | 1.32 | 0.01 | 0.106 | 0.001 |
| | | Mudstone | 450.0 | 13,311 | 118 | 1.23 | 0.02 | 49,358 | 224 | 1.17 | 0.01 | 0.270 | 0.003 |
| | | Mudstone | 460.0 | 11,676 | 112 | 1.27 | 0.02 | 39,275 | 200 | 1.18 | 0.01 | 0.297 | 0.003 |
| | | Mudstone | 470.0 | 5696 | 81 | 1.15 | 0.03 | 21,215 | 148 | 1.15 | 0.02 | 0.268 | 0.004 |
| | | Mudstone | 480.0 | 4573 | 74 | 1.15 | 0.04 | 17,536 | 135 | 1.12 | 0.02 | 0.261 | 0.005 |
| | | Mudstone | 490.0 | 4096 | 70 | 1.07 | 0.04 | 17,794 | 137 | 1.13 | 0.02 | 0.230 | 0.004 |
| | | Mudstone | 500.0 | 6885 | 88 | 1.21 | 0.03 | 293S0 | 174 | 1.14 | 0.01 | 0.234 | 0.003 |
| | | Mudstone | 510.0 | 9980 | 104 | 1.25 | 0.03 | 68,296 | 263 | 1.18 | 0.01 | 0.146 | 0.002 |
| | | Mudstone | 550.0 | 11,365 | | 1.21 | 0.02 | 45,110 | 214 | 1.15 | 0.01 | 0.252 | 0.003 |
| | | Mudstone | 569.7 | 13,853 | 121 | 1.24 | 0.02 | 63,171 | 253 | 1.19 | 0.01 | 0.219 | 0.002 |

**Table 3** continued

| Locality | GPS | Lithology | Height (cm) | IRSL | Error | IRSL depletion | Error | OSL | Error | OSL depletion | Error | IRSL/OSL ratio | Error |
|---|---|---|---|---|---|---|---|---|---|---|---|---|---|
| | | Mudstone | 632.9 | 7588 | 92 | 1.23 | 0.03 | 42,184 | 207 | 1.19 | 0.01 | 0.180 | 0.002 |
| | | Mudstone | 682.9 | 2900 | 62 | 1.18 | 0.05 | 16,437 | 132 | 1.25 | 0.02 | 0.176 | 0.004 |
| | | Mudstone | 710.9 | 4063 | 70 | 1.17 | 0.04 | 16,461 | 132 | 1.14 | 0.02 | 0.247 | 0.005 |
| | | Mudstone | 772.9 | 1886 | 52 | 1.08 | 0.06 | 6985 | 88 | 1.14 | 0.03 | 0.270 | 0.008 |
| | | Mudstone | 797.9 | 5677 | 81 | 1.20 | 0.03 | 22,551 | 154 | 1.14 | 0.02 | 0.252 | 0.004 |
| | | Mudstone | 1011.9 | 2291 | 56 | 1.05 | 0.05 | 12,176 | 114 | 1.26 | 0.02 | 0.188 | 0.005 |
| | | Mudstone | 1028.9 | 2088 | 54 | 1.02 | 0.05 | 9304 | 100 | 1.19 | 0.03 | 0.224 | 0.006 |
| | | Mudstone | 1,156.9 | 1804 | 52 | 1.08 | 0.06 | 5505 | 80 | 1.10 | 0.03 | 0.328 | 0.011 |
| | | Mudstone | 1,212.9 | 1885 | 52 | 1.11 | 0.06 | 5938 | 83 | 1.11 | 0.03 | 0.317 | 0.010 |
| | | Mudstone | 1,268.9 | 1792 | 52 | 1.06 | 0.06 | 5,955 | 83 | 1.21 | 0.03 | 0.301 | 0.010 |
| Section 5(a) Mcrsinlik OSL12-33A Kyrenia (Girne) terrace | N35 24.761′ E033 48.659′ | Mudstone | 0.0 | 13,066 | 119 | 1.22 | 0.02 | 121,384 | 350 | 1.21 | 0.01 | 0.108 | 0.001 |
| | | Mudstone | 200.0 | 6404 | 86 | 1.16 | 0.03 | 49,402 | 225 | 1.22 | 0.01 | 0.130 | 0.002 |
| | | Mudstone | 263.0 | 6036 | 85 | 1.50 | 0.04 | 45,541 | 216 | 1.24 | 0.01 | 0.133 | 0.002 |
| | | Mudstone | 294.0 | 6653 | 88 | 1.18 | 0.03 | 33,651 | 186 | 1.20 | 0.01 | 0.198 | 0.003 |
| | | Mudstone | 423.0 | 8308 | 98 | 1.23 | 0.03 | 36,084 | 193 | 1.20 | 0.01 | 0.230 | 0.003 |
| | | Mudstone | 522.0 | 13,982 | 123 | 1.28 | 0.02 | 80,612 | 285 | 1.24 | 0.01 | 0.173 | 0.002 |
| | | Mudstone | 599.0 | 8325 | 98 | 1.21 | 0.03 | 49,507 | 225 | 1.27 | 0.01 | 0.168 | 0.002 |
| | | Mudstone | 683.0 | 7871 | 95 | 1.21 | 0.03 | 31,459 | 180 | 1.16 | 0.01 | 0.250 | 0.003 |
| | | Mudstone | 763.0 | 5578 | 82 | 1.17 | 0.03 | 20,947 | 149 | 1.18 | 0.02 | 0.266 | 0.004 |
| | | Palaeosol | 838.0 | 3741 | 70 | 1.14 | 0.04 | 14,997 | 127 | 1.20 | 0.02 | 0.249 | 0.005 |
| | | Palaeosol | 874.0 | 3994 | 72 | 1.12 | 0.04 | 44,404 | 213 | 1.19 | 0.01 | 0.090 | 0.002 |
| | | Calcarenite | 922.0 | 5628 | 83 | 1.24 | 0.04 | 65,816 | 258 | 1.20 | 0.01 | 0.086 | 0.001 |
| | | Calcarenite | 948.0 | 5916 | 84 | 1.15 | 0.03 | 60,499 | 248 | 1.16 | 0.01 | 0.098 | 0.001 |
| | | Calcarenite | 987.0 | 6159 | 86 | 1.23 | 0.03 | 22,410 | 154 | 1.15 | 0.02 | 0.275 | 0.004 |
| | | Calcarenite | 1,037.4 | 10,760 | 109 | 1.18 | 0.02 | 18,246 | 139 | 1.09 | 0.02 | 0.590 | 0.007 |
| | | Calcarenite | 1,058.7 | 10,558 | 108 | 1.17 | 0.02 | 33,740 | 187 | 1.13 | 0.01 | 0.313 | 0.004 |
| | | Calcarenite | 1,103.0 | 26,550 | 167 | 1.31 | 0.02 | 43,140 | 210 | 1.13 | 0.01 | 0.615 | 0.005 |
| | | Calcarenite | 1,121.0 | 3963 | 71 | 1.15 | 0.04 | 17,387 | 137 | 1.16 | 0.02 | 0.228 | 0.004 |
| | | Calcaiviiilc | 1,140.0 | 14,215 | 124 | 1.24 | 0.02 | 34,963 | 190 | 1.15 | 0.01 | 0.407 | 0.004 |

The available petrographic information indicates that the relative mineralogical composition of the light-sensitive minerals (e.g. quartz; feldspar) remains relatively constant throughout the different sections sampled. This reflects the fact that the main source of the detrital minerals was the terrigenous sediments of the Kythrea (Değirmenlik) Group, which unconformably underlies the Quaternary terrace deposits along both flanks of the range. The composition of these deposits remains broadly similar throughout the Kyrenia Range, which reflects long-distance sedimentary transport from southern Turkey by gravity-flow processes (McCay and Robertson 2012).

A key observation is that the sections through the Kyrenia (Girne) and the Koupia terrace deposits exhibit very different averaged IRSL and OSL intensities. The Kyrenia (Girne) terrace deposits have signal intensities of between $10^3$ and $10^6$ photon counts, whereas the Koupia terrace deposits exhibit intensities generally greater than $10^6$ photon counts (Figs. 4, 5). Notably, the terrestrial deposits in the south show similar ranges in luminescence intensities to their inferred counterparts in the north (Fig. 9).

A number of discrete sedimentary units within the Kyrenia (Girne) and the Koupia terrace deposits are characterised by a specific set of luminescence features: (1) within the Kyrenia (Girne) terrace deposits, the net IRSL signal ranges between $10^4$ and $10^3$ photon counts in the aeolianites and between $10^5$ and $10^4$ photon counts in the marine deposits; (2) OSL signal intensities range between $10^5$ and $10^3$ photon counts in the aeolianites and between $10^5$ and $10^4$ photon counts in the marine deposits (Figs. 4, 5). Within the Koupia terrace deposits, the net IRSL signal ranges between $10^5$ and $10^4$ photon counts for the aeolian deposits, and $10^5$ photon counts for the marine deposits. OSL signal intensities are on the order of $10^5$ photon counts for both the aeolianites and the marine deposits.

The Kyrenia (Girne) fluvial terrace deposits on the northern flank of the range deposit exhibit IRSL signal intensities ranging from $10^4$ to $10^3$ photon counts. The OSL signal intensities are an order of magnitude higher than the IRSL signal intensities, ranging from $10^5$ to $10^4$ photon counts (Fig. 7). A similar order of magnitude difference is also recorded in the Kyrenia (Girne) terrace deposits on the southern side of the range (Section 6; Fig. 9). In addition, a number of discrete units can be distinguished based upon either normal or reversed signal patterns (Figs. 7, 9) on both sides of the range.

For the fluvial sections, the overall range in IRSL signal intensities is between $10^4$ and $10^3$ photon counts, and for OSL signal intensities, the range is between $10^6$ and $10^3$ photon counts (Figs. 7, 9). The aeolian calcarenites that overlie the fluvial sequence near Mersinlik have an IRSL intensity ranging from $10^3$ to $10^4$ photon counts; OSL signal intensities from this locality are c. $10^4$ photon counts (Fig. 7). The aeolianite signal intensities from the inland section are similar to the coastal aeolianites from the Kyrenia (Girne) terrace deposit.

Several packages of sediment can be identified within the luminescence profiles; these reflect marked changes in the luminescence signal intensity or a change from increasing to decreasing luminescence intensity or vice versa (Figs. 4, 5, 7 and 9). The packages are occasionally defined by lithological boundaries but generally do not correspond to identifiable changes in lithology. This suggests that the variation in the luminescence characteristics is due either to a variation in the depositional processes or to changes in the sediment provenance.

IRSL and OSL bleaching profiles for the Kyrenia (Girne) and the Koupia sediments are shown in Fig. 12. The IRSL and OSL signals are completely removed following 50 min of exposure (i.e. signal levels become indistinguishable from background levels): 70–80 % of the IRSL and OSL signals are lost within the first 30 min, and the remaining 30–20 % of signals are then lost in the following 60 min of exposure. This is promising luminescence behaviour, implying that the luminescence signals are susceptible to bleaching, suggesting that the material may have been well bleached at deposition. Interestingly, the bleaching profiles reveal a trend in bleaching susceptibility from the Kyrenia (Girne) aeolianites (easily bleached), through the Kyrenia (Girne) fluvial deposits, to the Koupia aeolianites, which are more difficult to bleach).

## Discussion and interpretation

The Kyrenia (Girne) terrace is 2–3 km wide and continuous for the c. 150 km length of the Kyrenia Range. In comparison, the Koupia terrace is <100 m wide and discontinuous along the length of the range. The Kyrenia (Girne) terrace deposits are 10–20 m thick, whereas the Koupia terrace deposits are <8 m thick.

Three depositional environments can be identified within the two terrace systems exposed near the northern coast: littoral marine, aeolian and fluvial. Each of these depositional environments is represented in both of the terrace systems. Both of the terrace systems on the northern side of the range exhibit an overall regressive sedimentary sequence.

The Kyrenia (Girne) terrace represents a variable, multi-facies depositional system. The succession generally begins with a basal conglomerate and passes upwards through shallow-marine calcarenites and then into coastal aeolianites. Fluvial deposits are channelled into the marine and aeolian deposits at various places along the length of the northern flank of the range. The

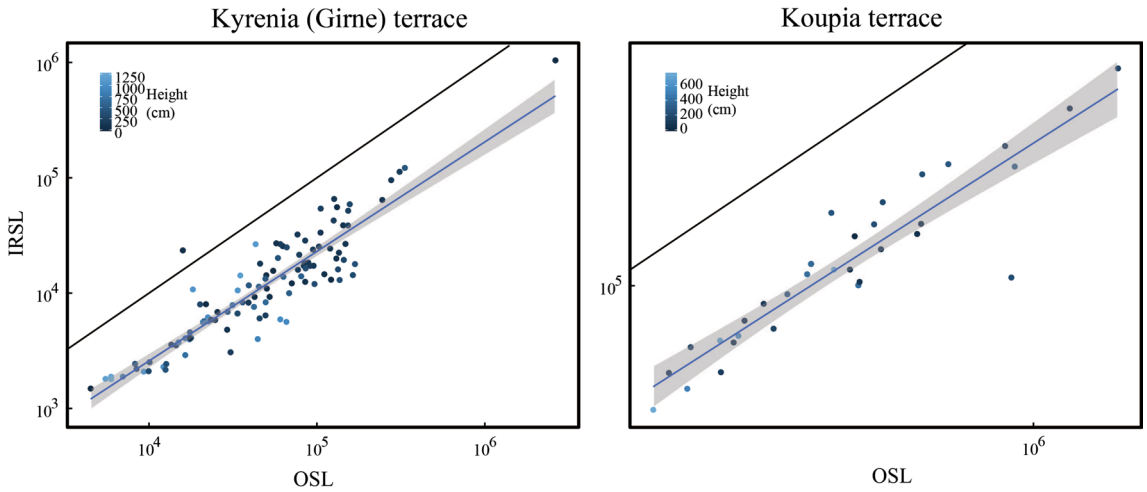


**Fig. 11** Scatter plots showing infrared stimulated luminescence (IRSL) versus optically stimulated luminescence (OSL). The heights shown by the shading of the dots for all of the Kyrenia (Girne) terrace samples on the left and all the Koupia terrace samples on the right. Both plots show that the IRSL and OSL signals in both terraces are directly interrelated. The OSL signal is generally higher than the IRSL signal, as shown by the offset of the data relative to the identity line

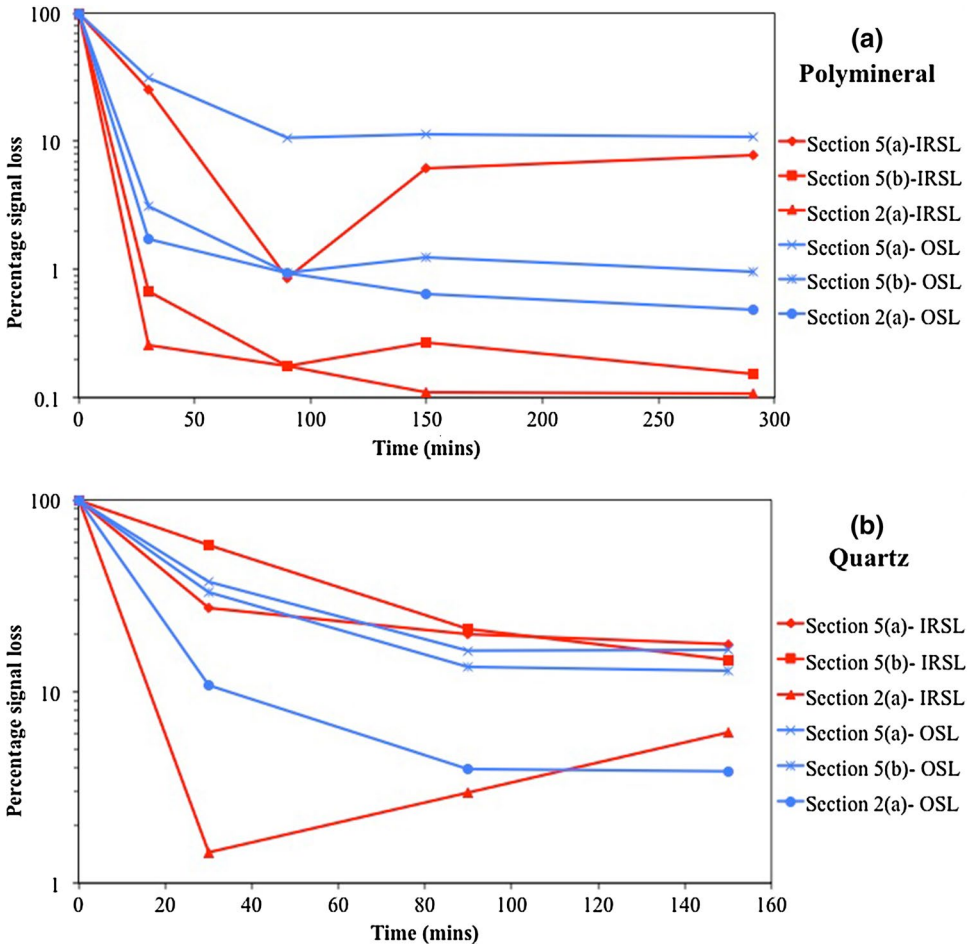


**Fig. 12** Bleaching data from polymineral and quartz aliquots averaged from Section 5(a), Section 5(b) and Section 2(a). The samples represent an even spread through each section. Samples were exposed under natural light conditions and then measured with the portable OSL reader at specific time intervals

uppermost component of the Kyrenia (Girne) terrace depositional system is an additional aeolianite that transgresses all of the other facies. In contrast, littoral marine and aeolianite depositional environments characterise the Koupia terrace system on the northern side of the range.

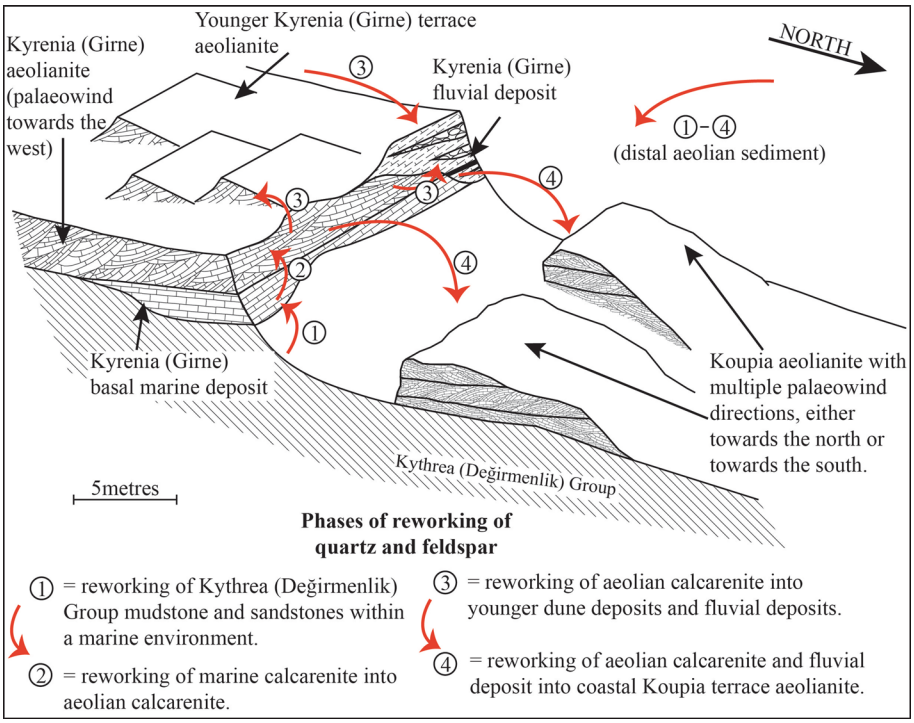


**Fig. 13** Schematic section based on field sedimentology and luminescence profiling, illustrating the sedimentary relationships and inferred phases of reworking of sediment between the Kyrenia (Girne) and the Koupia terrace deposits. The Kyrenia (Girne) terrace has a diverse range of depositional environments, from littoral marine to aeolianite and fluvial. The Koupia terrace is shown as patchy aeolianite that was deposited downslope of the Kyrenia (Girne) terrace

The terrace deposits along the southern flank of the range are exclusively non-marine. The southern-side terraces represent a series of crosscutting drainage systems. The southern-side drainage systems are deposited penecontemporaneously with the marine and continental terraces on the northern side of the range.

The Koupia deposits are known to be younger than the Kyrenia (Girne) terrace deposits along both the northern and southern flanks of the range. This is mainly because the younger sediments are seen to depositionally overlie or crosscut the older sediments at many locations. Although absolute ages are not yet available for the two terrace systems, the Koupia terrace deposits appear to represent a much shorter time interval than the Kyrenia (Girne) terrace deposits. This is because the Koupia deposits are thinner, more homogeneous and localised along the coast in contrast to the Kyrenia (Girne) deposits, which are thicker, lithologically more variable, form episodically and extend as transgressive sheets up to several kilometres inland. The inference that the Kyrenia (Girne) terrace represents a longer period of time than the Koupia terrace is supported by the luminescence proxy data. Not withstanding the different lithological units, depositional mechanisms, and environmental setting of the two terrace systems, there is a greater range in signal intensities within the Kyrenia (Girne) terrace than the Koupia terrace.

The ages of the sediments in the different sections of the terrace can be inferred to be broadly similar in cases where the luminescence signals are similar. On this basis, the distributions of the Kyrenia (Girne) terrace deposits and the Koupia terrace deposits that were originally recognised based on regional mapping of associated geomorphological surfaces (Ducloz 1963; Knupp 1964) are now generally confirmed from the combination of sedimentological and optical luminescence data presented here. In addition, the fluvial terraces on the southern flank of the range can now be correlated within mixed marine/non-marine terraces in at least two different sections.

The luminescence profiles through the fluvial terraces on the northern side of the range are indicative of three sediment packages with specific luminescence characteristics (Figs. 7, 9). The packages represent sediment that underwent subtly different sedimentary histories, resulting in subtly differently luminescence signals. The different packages of sediment are likely to be the product of an episodically changing depositional system.

The IRSL and OSL intensities show a progression from the largest intensities at the base to the lowest intensities at the top. This is expected for a normal age progression in which lower, stratigraphically older sediments have had longer to accumulate luminescence signals in situ. The relative decrease in the luminescence intensity of each section suggests that, within individual sections, the primary control of luminescence intensity is likely to be age.

The Kyrenia (Girne) and Koupia terrace deposits on the northern side of the range are characterised by specific luminescence characteristics. The Kyrenia (Girne) terrace deposits have IRSL intensities of between $10^4$ and $10^3$ photon counts, whereas the Koupia terrace IRSL signal intensities range from $10^6$ to $10^5$ photon counts. The Kyrenia

**Table 4** IRSL, OSL and depletion data, with associated errors, for the Kyrenia (Girne) and Koupia terrace fluvial deposits on the southern side of the Kyrenia Range

| Locality | GPS | Lithology | Height (cm) | IRSL | Error | IRSL depletion | Error | OSL | Error | OSL depletion | Error | IRSL/OSL ratio | Error |
|---|---|---|---|---|---|---|---|---|---|---|---|---|---|
| Section 6 Kalkanh (Kapouti) OSL 12-31 Kyrenia (Girne) terrace | N35 15.168′E033 02.830′ | Mudstone | 23.0 | 4035 | 69 | 1.19 | 0.04 | 17,524 | 135 | 1.13 | 0.02 | 0.230 | 0.004 |
| | | Mudstone | 89.0 | 4813 | 75 | 1.19 | 0.04 | 29,195 | 173 | 1.18 | 0.01 | 0.165 | 0.003 |
| | | Mudstone | 152.0 | 5844 | 81 | 1.20 | 0.03 | 24,762 | 160 | 1.16 | 0.01 | 0.236 | 0.004 |
| | | Mudstone | 184.0 | 3068 | 62 | 1.17 | 0.05 | 30,591 | 177 | 1.46 | 0.02 | 0.100 | 0.002 |
| | | Mudstone | 214.0 | 5882 | 82 | 1.17 | 0.03 | 23,404 | 155 | 1.14 | 0.02 | 0.251 | 0.004 |
| | | Mudstone | 288.9 | 2103 | 54 | 1.12 | 0.06 | 9952 | 104 | 1.16 | 0.02 | 0.211 | 0.006 |
| | | Mudstone | 331.4 | 2517 | 57 | 1.12 | 0.05 | 10,073 | 105 | 1.12 | 0.02 | 0.250 | 0.006 |
| | | Mudstone | 368.6 | 2428 | 57 | 1.09 | 0.05 | 12,665 | 116 | 1.18 | 0.02 | 0.192 | 0.005 |
| | | Mudstone | 407.6 | 2165 | 54 | 1.05 | 0.05 | 12,541 | 115 | 1.23 | 0.02 | 0.173 | 0.005 |
| | | Mudstone | 442.8 | 2435 | 57 | 1.17 | 0.05 | 8258 | 95 | 1.13 | 0.03 | 0.295 | 0.008 |
| Section 7 Nergisli (Genagra) OSL12-32 Koupia terrace | N35 13.198′E035 13.198′ | Mudstone | 34.9 | 151,478 | 391 | 1.26 | 0.01 | 534,027 | 731 | 1.05 | 0.003 | 0.284 | 0.001 |
| | | Mudstone | 91.3 | 63,430 | 254 | 1.27 | 0.01 | 198,633 | 447 | 1.15 | 0.01 | 0.319 | 0.001 |
| | | Mudstone | 108.8 | 49,970 | 226 | 1.25 | 0.01 | 185,461 | 432 | 1.13 | 0.01 | 0.269 | 0.001 |
| | | Mudstone | 198.9 | 106,812 | 328 | 1.33 | 0.01 | 887,413 | 942 | 1.11 | 0.002 | 0.120 | 0.000 |
| | | Mudstone | 256.4 | 179,427 | 425 | 1.31 | 0.01 | 336,352 | 581 | 1.11 | 0.004 | 0.533 | 0.002 |

(Girne) terrace OSL intensities are $10^5$ to $10^4$ photon counts, whereas the Koupia terrace intensities are $10^6$ to $10^5$ photon counts. The IRSL and OSL signal intensities therefore indicate an order of magnitude difference between the Kyrenia (Girne) and Koupia terrace deposits. A similar pattern of hugely different luminescence signals is present within the two terraces studied along the southern flank of the range. Given the known stratigraphic and sedimentological relationships between the terraces, this relationship must be due to some combination of differences in mineralogy, depositional process and/or diagenesis, all of which could affect internal luminescence characteristics. As noted earlier, the petrographical evidence does not indicate any major difference in mineralogy between the two terrace systems, although local differences exist within and between individual sections. The contrasts in signal intensity encompass a range of depositional environments within both the Kyrenia (Girne) and Koupia terrace systems, suggesting that the luminescence differences are not facies dependent.

A further factor that could explain the intensity relationship is the sensitivity (i.e. efficiency) of the sediment incorporated into each terrace. The intensity of the OSL signal from a quartz grain is a function of the size of the total radiation exposure to which it has been exposed since burial (luminescence in growth), together with the efficiency with which this radiation dose is expressed as emitted photons during the measurement process. This efficiency (sensitivity) varies between quartz types and may also vary within a single type of quartz grain depending upon the number of phases of deposition and reworking (Pietsch et al. 2008). Sedimentary processes can influence the sensitivity of a deposit, i.e. the sensitivity tends to increase with additional phases of deposition and reworking (Pietsch et al. 2008). The high signal associated with the Koupia terrace could have been caused by a high sensitivity that resulted from multiple phases of sediment reworking from the Kyrenia (Girne) terrace into the Koupia terrace.

Figure 13 shows a schematic model to account for the phases of reworking, depositional pathways and potential sediment sources of the two terrace deposits. The Kyrenia (Girne) terrace is a multi-phase system with a basal marine calcarenite, overlain by an aeolianite, which has been subsequently down-cut into by a fluvial system; finally in some areas, this entire sequence was overlain by a younger aeolianite. In contrast, the Koupia terrace is represented by a single relatively simple phase of aeolian deposition. The Eocene–Miocene Kythrea (Değirmenlik) Group is the main source of the identifiable quartz and feldspar within the two terrace deposits. The luminescence characteristics of the two sediment deposits are very different, which could be a consequence of the different sedimentary histories. Figure 13 illustrates the reworking of sediment from the Kythrea (Değirmenlik) Group into the Kyrenia (Girne)

**Table 5** Background gamma readings for five Kyrenia (Girne) and Koupia terrace deposits

| Locality | Height (cm) | Gamma (m/Ga) | Error | Lithology |
|---|---|---|---|---|
| Section 1 OSL12-29 Kyrenia (Girne) terrace | 0.0 | 0.44 | 0.013 | Marine calcarenite |
| | 130.0 | 0.36 | 0.010 | Marine calcarenite |
| | 250.0 | 0.43 | 0.011 | Aeolian calcarenite |
| Section 5(b) (OSL12-20) Koupia terrace | 0.0 | 0.55 | 0.011 | Aeolian calcarenite |
| | 400.0 | 0.71 | 0.011 | Aeolian calcarenite |
| | 500.0 | 0.62 | 0.010 | Aeolian calcarenite |
| | 700.0 | 0.89 | 0.016 | Aeolian calcarenite |
| Section 5(a) (OSL12-33A) Kyrenia (Girne) terrace | 200.0 | 1.77 | 0.028 | Palaeosol |
| | 423.0 | 0.48 | 0.009 | Mud |
| | 922.0 | 1.08 | 0.019 | Palaeosol |
| | 1037.4 | 0.55 | 0.010 | Aeolian calcarenite |
| Section 6 (OSL12–31) Kyrenia (Girne) terrace | 0.0 | 0.32 | 0.016 | Mud |
| | 200.0 | 1.04 | 0.016 | Mud |
| | 450.0 | 0.31 | 0.017 | Mud |
| Section 7 (OSL12–32) Koupia terrace | 0.0 | 0.68 | 0.011 | Sand |
| | 100.0 | 0.55 | 0.009 | Sand |
| | 200.0 | 0.72 | 0.011 | Sand |

See Fig. 2 for locations of the sections

terrace deposits and finally into the Koupia aeolianites. The first phase of reworking involved the initial erosion of the Kythrea (Değirmenlik) Group into the calcarenite at the base of the Kyrenia (Girne) terrace within a marine environment. The second phase indicates the erosion of the Kyrenia (Girne) marine calcarenite into the overlying beach and dune deposits. Phase three shows the erosion of the oldest Kyrenia (Girne) terrace aeolianite in response to fluvial down-cutting into younger dune systems. The final fourth phase shown is the erosion of all of the deposits into the coastal Koupia terrace aeolianite. The sediment that was finally deposited in the Koupia terrace, therefore, potentially experienced at least four phases of reworking and redeposition. A comparable process can also be envisaged for the southern side of the Kyrenia Range in which multiple phases of fluvial reworking took place from the Kyrenia (Girne) deposits to the Koupia deposits. The end product of such processes would be a much higher sensitivity of the quartz and feldspar grains within topographically the lower terrace compared with the higher terrace, finally resulting in the higher observed IRSL and OSL signal intensities in the younger terrace deposits.

## Conclusions

A combination of sedimentology and portable OSL data provides a good understanding of the evolving depositional environments of the Kyrenia (Girne) and Koupia terrace systems. On the northern flank of the Kyrenia Range, both terraces represent an overall regressive sedimentary sequence, with the Kyrenia (Girne) terrace deposits being much more diverse than those of the Koupia terrace system. The terrestrial component within the Kyrenia (Girne) terrace comprises a combination of fluvial and aeolian deposits.

The portable OSL reader facilitated the rapid analysis of 107 samples, enabling comparisons within and between the individual sediment packages on both flanks of the Kyrenia Range. IRSL and OSL intensities are distinct for each terrace, allowing a quantitative correlation of the terrace deposits on the northern and southern sides of the range. Furthermore, the IRSL and OSL intensity profiles are suggestive of multiple depositional episodes with different packages of sediment showing contrasting luminescence characteristics. The luminescence profiles through the fluvial deposits on both flanks of the range are consistent with sedimentary interpretations of an episodically changing depositional system. The luminescence profiles suggest that the fluvial system represents up to three or four major phases of deposition. The specific luminescence characteristics show that the different terrace deposits in spatially distinct and separate areas can be confidently correlated for the first time.

The net signal intensities obtained for the younger, Koupia terrace sediments are generally an order of magnitude larger than those in the older, Kyrenia (Girne) deposits. The differences in signal intensity may be explained by multiple episodes of reworking of the Kyrenia (Girne) terrace deposits, which increased the sensitivity of the sediment and thereby resulted in the higher intensities in the Koupia terrace luminescence profiles.

The luminescence characteristics of the marine to non-marine Quaternary terrace deposits, as obtained using the portable OSL reader, can be used to laterally correlate the different terrace sedimentary sequences on both the northern and southern flanks of the Kyrenia Range. Field luminescence profiles can be used in tandem with field sedimentary information to help interpret the depositional processes. Absolute dating is in progress to further constrain the relative ages of the different terrace depositional systems.

## References


Bagnall PS (1960) The Geology and Mineral Resources of the Pano Lefkara-Larnaca Area. Geol. Surv. Depart. Cyprus, Memoir, 5, 116

Baroz F (1979) Étude géologique dans le Pentadaktylos et la Mesaoria (Chypre Septentrionale). Earth Sciences. Nancy, Université de Nancy. Unpubl. PhD thesis

Burbidge CI, Sanderson DCW, Housley RA, Allsworth JP (2007) Survey of Palaeolithic sites by luminescence profiling, a case study from Eastern Europe. Quat Geochronol 2(1):296–302

Constantinou G (1995) Geological map of Cyprus. Technical report, Geol SurDept, Cyprus

Cosentino D, Schildgen TF, Cipollari P, Faranda C, Gliozzi E, Hudácková N, Lucifora S, Strecker MR (2011) Late miocene surface uplift of the Southern margin of the central anatolian plateau, central taurides, Turkey. Geol Soc Am Bull 124:133–145

Dilek Y, Sandvol E (2009) Seismic structure, crustal architecture and tectonic evolution of the Anatolian–African Plate Boundary and the Cenozoic Orogenic Belts in the Eastern Mediterranean Region. In Murphy JB, Keppie JD, Hynes AJ (eds) 2009. Ancient Orogens and Modern Analogues. Geol Soc London, Spec Publ. 327:127–160

Dreghorn W (1978) Landforms in the Girne Range Northern Cyprus. Ankara, Maden Tetkik ve Arama Enstitüsü, Ankara, Turkey

Ducloz C (1963) Geological map of the Central Kyrenia Range. Geol Surv Dept., Cyprus

Ducloz C (1964) Revision of the pliocene and Quaternary stratigraphy of the central Mesaoria. The Cosmos Press Ltd, Nicosia Cyprus, Nicosia

Ducloz C (1972) The geology of the bellapais-kyrthrea area of the central Kyrenia range. Bull. 6. Geol Surv Dept Nicosia, Cyprus

Durcan JA, Roberts HM, Duller GAT, Alizai AH (2010) Testing the use of range-finder OSL dating to inform field sampling and laboratory processing strategies. Quat Geochronol 5(2):86–90

Frébourg G, Hasler C-A, Guern PL, Davaud E (2008) Facies characteristics and diversity in carbonate eolianites. Facies 54(2):175–191

Garzanti E, Andò S, Scutellà M (2000) Actualistic ophiolite provenance: the Cyprus case. J Geol 108:199–218

Göğüş OH, Pysklywec RN (2008) Mantle lithosphere delamination driving plateau uplift and synconvergent extension in eastern Anatolia. Geology 36(9):723–726

Harrison RW, Newell WL (2004) Tectonic framework and late Cenozoic tectonic history of the northern part of Cyprus: implications for earthquake hazards and regional tectonics. J Asian Earth Sci 23:91–210

Harrison RW, Tsiolakis E, Stone BD, Lord A, Mcgeehin JP, Mahan SA, Chirico P (2012) Late pleistocene and holocene uplift history of Cyprus: implications for active tectonics along the southern margin of the Anatolian microplate. In: Robertson AHF, Parlak O, Ünlügenç UC (eds) 2012. Geological development of Anatolia and the Easternmost Mediterranean Region. Geol Soc London Spec Publ 372(1):561–584

Henson FRS, Browne RV, McGinty J (1949) A synopsis of the stratigraphy and geological history of Cyprus. Q J G S 105:1–41

Jaffey M, Robertson AHF (2004) Non-marine sedimentation associated with oligocene-recent exhumation and uplift of the Central Taurus Mountains, S. Turkey. Sedim Geol 173:53–89

Kempler D, Ben-Avraham Z (1987) The tectonic evolution of the Cyprean Arc. Ann Tecton 1:58–71

Kinnaird T, Robertson AHF (2013) Tectonic and sedimentary response to subduction and incipient continental collision in southern Cyprus, easternmost Mediterranean region. In: Robertson AHF, Parlak O, Ünlügenç UC (eds) 2013. Geological Development of Anatolia and the Easternmost Mediterranean Region. Geol Soc Lond Spec Pub 372(1):585–614

Kinnaird TC, Robertson AHF, Morris A (2011) Timing of uplift of the troodos massif (Cyprus) constrained by sedimentary and magnetic polarity evidence. J Geol Soc London 168:457–470

Kinnaird TC, Sanderson D, Woodward N (2012) Applying luminescence methods to geo-archaeology: a case study from Stronsay, Orkney. Trans R Soc Edinburgh Earth Sci 102:191–199

Knupp C (1964) Geological map of the Central Kyrenia Range. Geol Surv Dept. Nicosia, Cyprus

Leeder MR, McNeill LC, Collier REL, Portman C, Rowe PJ, Andrews JE (2003) Corinth rift margin uplift: new evidence from late quaternary marine shorelines. J Geophy Res 30(12):1611

Lian OB, Roberts GR (2006) Dating the Quaternary: progress in luminescence dating of sediments. Quatern Sci Rev 25(19–20):2449–2468

McCallum JE, Robertson AHF (1995a) Sedimentology of the two fan-delta systems in the Pliocene-Pleistocene of the Mesaoria Basin Cyprus. Sed Geol 98:215–244

McCallum JE, Robertson AHF (1995b) Late Miocene-Early Pleistocene Athalassa Formation, north central Cyprus: carbonate sand bodies in a shallow seaway between two emerging landmasses. Terra Nova 7:265–277

McCay GA, Robertson AHF (2012) Sedimentology and provenance of Upper Eocene-Upper Miocene clastic sediments of the Girne (Kyrenia) Range, northern Cyprus: a case history of sedimentation related to progressive and diachronous continental collision. Sed Geol 265:30–55

McCay GA, Robertson AHF, Kroon D, Raff I, Ellam RM, Necdet M (2012) Stratigraphy of cretaceous to lower pliocene sediments in the northern part of Cyprus based on comparative $^{87}Sr/^{86}Sr$ isotopic nannofossil and planktonic foraminiferal dating. Geol. Mag. 1–27

Moshkovitz S (1966) The age of the Kyrenia Formation in Cyprus 2. In: International Union of Geologial Sciences, Proc. 3rd Session, Berne 303

Muñoz-Salinas E, Bishop P, Sanderson DCW, Zamorano J-J (2011) Interpreting luminescence data from a portable OSL reader: three case studies in fluvial settings. Earth Surf Proc Land 36:651–660

Munyikwa K, Brown S, Kitabwalla Z (2012) Delineating stratigraphic breaks at the bases of postglacial eolian dunes in central Alberta, Canada using a portable OSL reader. Earth Surf Proc Land 37(15):1603–1614

Necdet M, Anıl M (2006) The geology and geochemistry of the gypsum deposits in Northern Cyprus. Geosound (Yerbilimleri) 48–49:11–49

Palamakumbura RN (2015) Sedimentary, geomorphological and dating evidence for the uplift of the Kyrenia Range, northern Cyprus: testing alternative regional tectonic models. Unpublished PhD thesis. University of Edinburgh

Pietsch TJ, Olley JM, Nanson GC (2008) Fluvial transport as a natural luminescence sensitiser of quartz. Quat Geochronol 3(4):365–376

Poole A, Robertson AHF (1991) Quaternary uplift and sea-level change at an active plate boundary, Cyprus. J Geol Soc London 148(5):909–921

Poole AJ, Robertson AHF (1998) Pleistocene fanglomerates deposition related to uplift of the Troodos Ophiolite, Cyprus. In: Robertson, A.H.F., Emeis, K.-C., Richter, C., Camerlenghi, A. (eds), Proc ODP Scientific Results. 160:544–568

Poole AJ, Robertson AHF (2000) Quaternary marine terraces and aeolianites in coastal south and west Cyprus: implications for regional uplift and sea-level change. In: Panayides I. Xenophontos C., Malpas J (eds). Proc 3rd Internat Conf on the geology of the Eastern Mediterranean. Cyprus Geol Surv. Dert Nicosia, Cyprus

Poole A, Shimmield G, Robertson AHF (1990) Late Quaternary uplift of the Troodos ophiolite, Cyprus: uranium-series dating of Pleistocene coral. Geology 18:894–897

Reed FR (1930) Contributions to the geology of Cyprus. Geol Mag 76(06):241–271

Reed FR (1935) Notes on the neogene faunas of Cyprus. The pliocene faunas. J Nat Hist 16(95):489–524

Rhodes EJ (2011) Optically stimulated luminescence dating of sediments over the past 200,000 years. Ann Rev Earth Planet Sci 39:461–488

Roberts HM, Duller GA (2004) Standardised growth curves for optical dating of sediment using multiple-grain aliquots. Radiat Meas 38(2):241–251

Roberts HM, Durcan JA, Duller GA (2009) Exploring procedures for the rapid assessment of optically stimulated luminescence rangefinder ages. Radiat Meas 44(5):582–587

Robertson AHF (1990) Tectonic evolution of Cyprus. In: Malpas J, Moores E, Panayiotis A, Xenophontos C. Ophiolites-oceanic crustal analogues. ProcSymp 'Troodos 1987′, Geol Surv Depart, Cyprus, 235–253

Robertson AHF (1998) Tectonic significance of the Eratosthenes Seamount: a continental fragment in the process of collision with a subduction zone in the eastern mediterranean (Ocean drilling program leg 160). Tectonophysics 298:63–82

Robertson AHF (2000) Tectonic evolution of Cyprus in its Easternmost Mediterranean setting. In: Panayides I, XenophontosC, Malpas J. (Eds), Proc 3rd Internat Conf on the Geology of the Eastern Mediterranean, Geoll SurvDept Cyprus, 11–44

Robertson AHF, Woodcock NH (1986) The role of the Kyrenia Range Lineament, Cyprus, in the geological evolution of the Eastern Mediterranean area. Phil. Trans. R. Soc. London. Series A, Mathematical and Physical Sciences, In: Reading HG, Watterson J, White, SH. 1987. Major Crustal Lineaments and their influences on the Geological History of Continental Lithosphere 317 (1539):141–177

Robertson AHF, Tasli K, İnan N (2012) Evidence from the Kyrenia Range, Cyprus, of the northerly active margin of the Southern Neotethys during Late Cretaceous-early Cenozoic time. Geol Mag 149(02):1–27

Robertson AHF, McCay GA, Taslı K, Yıldız A (2014) Eocene development of the northerly active continental margin of the Southern Neotethys in the Kyrenia Range, north Cyprus. Geol Mag 151(4):692–731

Sanderson DCW, Murphy S (2010) Using simple portable OSL measurements and laboratory characterization to help understand complex and heterogeneous sediment sequences for luminescence dating. Quat Geochronol 5:299–305

Sanderson DCW, Bishop P, Houston I, Boonsener M (2001) Luminescence characterisation of quartz-rich cover sands from NE Thailand. Quatern Sci Rev 20(5):893–900

Sanderson DCW, Bishop P, Stark MT, Spencer JQ (2003) Luminescence dating of anthropogenically reset canal sediments from Angkor Borei, Mekong Delta, Cambodia. Quatern Sci Rev 22(10):1111–1121

Schildgen TF, Cosentino D, Bookhagen B, Niedermann S, Yıldırım C, Echtler H, Wittmann H, Strecker MR (2012) Multi-phased uplift of the Southern margin of the central anatolian plateau, Turkey: a record of tectonic and upper mantle processes. Earth Planet Sci Lett 317–318:85–95

Hakyemez Y, Turhan N, Sönmez, İ, Sümengen M (2000) Kuzey Kıbrıs Türk Cumhuriyeti' nin Jeolojisi, MTA. Genel Müdürlüğü Jeoloji Etütleri Diaresi, Ankara: 44

Weber J, Schirmer W, Heller F, Bachtadse V (2011) Magnetostratigraphy of the Apalós Formation (early Pleistocene): evidence for pulsed uplift of Cyprus. Geochemistry, Geophysics, Geosystems 12 (1)

Weiler Y (1970) Mode of occurrence of pelites in the Kythrea Flysch Basin (Cyprus). J Sed Petrol 40:1255–1261

Zomeni Z (2012) Quaternary marine terraces on Cyprus: constraints on uplift and pedogenesis, and the geoarchaeology of Palaipafos. Unpublished PhD thesis. Oregon State University